

Water Resources Research®

RESEARCH ARTICLE

10.1029/2024WR037454

Key Points:

- Evapotranspiration becomes less sensitive to precipitation variability as canopy density increases in Taiga Shield forests
- Taiga vegetation tends to draw younger less evaporatively enriched soil water, and denser forests tend to have older more evaporatively enriched water in soils by the end of the growing season
- Increased forest cover is not expected to change catchment water cycles because open water and exposed bedrock restrict tree expansion

Correspondence to:

C. Spence,
chris.spence@ec.gc.ca

Citation:

Spence, C., Coles, A., Gibson, J. J., Nicholls, E. M., Perron, N., Sniderhan, A., et al. (2024). The influence of tree infilling on energy partitioning, vegetation water use, and soil water state in sparse conifer stands of the Taiga Shield ecoregion. *Water Resources Research*, 60, e2024WR037454. <https://doi.org/10.1029/2024WR037454>

Received 8 MAR 2024

Accepted 24 JUL 2024

© 2024 His Majesty the King in Right of Canada and The Author(s). Reproduced with the permission of the Minister of Environment and Climate Change Canada. This is an open access article under the terms of the [Creative Commons Attribution-NonCommercial-NoDerivs License](https://creativecommons.org/licenses/by/4.0/), which permits use and distribution in any medium, provided the original work is properly cited, the use is non-commercial and no modifications or adaptations are made.

The Influence of Tree Infilling on Energy Partitioning, Vegetation Water Use, and Soil Water State in Sparse Conifer Stands of the Taiga Shield Ecoregion

C. Spence¹ , A. Coles², J. J. Gibson³ , E. M. Nicholls¹ , N. Perron⁴ , A. Sniderhan⁵ , O. Sonnentag⁴ , and J. L. Baltzer⁵ 

¹Environment and Climate Change Canada, Saskatoon, SK, Canada, ²Government of the Northwest Territories Environment and Natural Resources, Yellowknife, NT, Canada, ³Innotech Alberta, Victoria, BC, Canada, ⁴Université de Montréal, Montréal, QC, Canada, ⁵Wilfrid Laurier University, Waterloo, ON, Canada

Abstract Climate warming and permafrost thaw induced land cover change are well documented in much of the circumpolar north. The extensive exposure of Precambrian continental crust in Canada's Taiga Shield ecoregion could mean impacts of land cover change documented in other regions without this feature are not transferable. This study examined energy partitioning with eddy covariance measurements, vegetation water use with stable isotopes and soil water state with time domain reflectometry sensors in conifer stands in the Taiga Shield ecoregion. The goal was to determine how changes in forest density with climate warming could influence water budget response and soil water state. Paired measurements of sensible and latent heat imply evaporative processes in denser canopies are controlled more by radiative than the aerodynamic factors predominant in sparser canopies. As denser canopies become more prevalent on the landscape, this switch in relative importance of evapotranspirative processes will lead to a reduction in inter-annual variability of evapotranspiration. The dominant tree species (black spruce, tamarack and jack pine) were all quick to draw water from shallow soils after spring thaw and rainfall. Stand structural changes resulted in older, more evaporatively enriched water prevalent in soils below dense canopies. While there is evidence for forest infilling, widespread lakes and exposed bedrock restricts extensive expansion of forested land covers. The insufficient difference between sparse and dense canopy evapotranspiration suggest a fundamental change in how water cycles in Taiga Shield catchments is unlikely, which is notably different than previously investigated landscapes in Alaska and the Canadian Taiga Plains.

1. Introduction

Climate warming of $\sim 0.6^\circ\text{C}$ per decade across the northern circumpolar region over the last half century is unequivocal (Box et al., 2019). Associated with this warming have been coincident changes in vegetation productivity due to altered growing conditions (Chapin et al., 2005; Elmendorf et al., 2012; Travers-Smith & Lantz, 2020), enhanced wildfire activity (Baltzer et al., 2021; Heim et al., 2021) and landscape change with permafrost thaw and loss (Jorgenson et al., 2008; Kokelj et al., 2023; Lantz et al., 2013). Away from range margins such as alpine and arctic treelines, species composition (Reid et al., 2021) and canopy density (Sniderhan et al., 2023) are responding to climate warming, with canopies infilling because of longer warmer growing seasons while simultaneously seeing compositional changes in response to drought, insects and fire (Foster et al., 2022). These widespread changes bring a growing need to understand how changes in canopy structure and composition influence partitioning of the water cycle and alter flow paths, water sources and quantity and timing of fluxes (Brooks et al., 2015; Tetzlaff et al., 2021).

Empirical data that show how denser subarctic vegetation canopies influence evapotranspiration rates are uncommon (e.g., Nicholls & Carey, 2021) and are mostly limited to effects of shrubification (Endrizzi & Marsh, 2010; Sturm et al., 2005; Wilcox et al., 2022). Feedbacks are expected with atmospheric conditions since vegetation cover responds to climate warming (Bonan, 2008). Because landscape patches in the boreal forest are often unevenly organized over distances of < 10 km (Garratt, 1994), the planetary boundary layer tends to be well mixed. Incoming radiation, vapor pressure deficit (VPD) and air temperature tend to be similar among nearby patches of different small-scale (1–10 ha) landscape components (Oke, 1987). At this scale, land surface characteristics such as albedo and ecophysiological attributes (e.g., canopy resistance) should be those responsible for any differences in evapotranspiration rates (Helbig et al., 2016; Kasurinen et al., 2014).

The influence of forest ecophysiological attributes on the division of the energy budget varies in high latitude systems. Assessing a variety of sites across the Canadian Taiga, Eaton et al. (2001) found the ratio of latent heat flux to net radiation (Q_e/Q^*) is inversely related to subarctic vegetation canopy density. This is opposite to what Nicholls and Carey (2021) found along an elevation and vegetation gradient in a montane catchment in southwest Yukon, Canada. Since evapotranspiration is a combination of over and understory transpiration, evaporation of intercepted water, and ground evaporation, resultant values of Q_e/Q^* will depend on the relative size of each flux. There is some counterintuitive evidence that more trees may reduce canopy-scale evapotranspiration by reducing available energy to the understory (Thompson, 2012) which in subarctic canopies accounts for 50%–80% of evapotranspiration (Blanken et al., 2001; Eugster et al., 2000; Iida et al., 2009; Lafleur, 1992; R. K. Warren et al., 2018). Black spruce (*Picea mariana*), the most common and widespread tree species in the Canadian Taiga (Viereck & Johnston, 1990), typically have low transpiration rates (R. K. Warren et al., 2018). Thus, higher overstory transpiration may be insufficient to counteract reductions in subcanopy rates with increasing tree density, leading to an overall decrease in ecosystem-scale evapotranspiration. Kettridge et al. (2013) and Lafleur and Humphreys (2018) found the canopy density-latent heat flux relationship to be nonlinear because the sources of water for evapotranspiration among canopy components can be so diverse, especially as wetness conditions change through time. So, the range of observations of Q_e/Q^* documented by Eaton et al. (2001) and Nicholls and Carey (2021) could be due to the wide range in over- and understory densities that occur in the subarctic (Grelle et al., 1997).

These shifts in the relative rates of surface evaporation and transpiration presumably change the source of water used to supply each, which may impact vadose zone hydrology (Botter et al., 2010; Penna et al., 2018; Sprenger, Tetzlaff, Buttle, Carey, et al., 2018; Tetzlaff et al., 2013). The boreal forest canopy is comprised of species that operate along a gradient of water use and stomatal regulation strategies (McDowell et al., 2008). Two of the most common species, tamarack (*Larix laricina*) and black spruce, can employ very different water use strategies (J. M. Warren et al., 2021). These differences in hydraulic strategies may mean different soil water sources, ages and residence times associated with varying canopy compositions (Nehemy et al., 2021, 2022), but results are ambiguous among ecozones. These differences can appear very early in the growing season. Previously, trees were assumed dormant during snowmelt because cold soils restrict root uptake, reduce leaf turgor and force stomatal closure (Baldocchi et al., 2000; Halldin et al., 1980). More recently, Young-Robertson et al. (2016) and Nehemy et al. (2022) have shown that boreal tree species access water at different rates immediately following snowmelt. As the growing season begins and progresses, soil water composition continues to evolve due to evapotranspiration, but this can be tempered depending on relative rates of precipitation, transpiration, and evaporation (Snelgrove et al., 2021), vegetation type, soil properties, and landscape position (Geris et al., 2017). Modeling studies imply antecedent precipitation can be a stronger driver than potential evaporation on dynamics of isotopes in soil waters (Sprenger, Tetzlaff, Buttle, Laudon, & Soulsby, 2018). This may be because subarctic plant species are likely opportunistic and use available water with no preference or discrimination (Nicholls & Carey, 2021).

A notable knowledge gap is how changes in vegetation density will alter soil water conditions (i.e., content, age, and resultant water chemistry) in the taiga where forest infilling is occurring rapidly in response to high latitude warming (Helbig et al., 2016). Densification of the tree canopy could have implications for aquatic chemistry as soil water residence times change. Previous studies are somewhat limited in geographic scope with almost all work taking place in Boreal and Taiga Plains ecoclimatic regions, leaving the Taiga Shield landscapes that occur in Canada, Scandinavia, and Russia understudied (Wright et al., 2022). Furthermore, there are no upscaling studies to determine the extent to which tree canopies need to densify to create a detectable catchment-scale response in evapotranspiration rates, especially where underlying surficial geology may play a strong role. In this study, we address two questions; (a) how does canopy density in the Taiga Shield influence (a) energy partitioning, (b) sources of vegetation water use, and (c) soil water state (i.e., age and content) as well as (b) how much canopy infilling is needed to create measurable changes in evapotranspiration rates at the catchment scale?

2. Study Area and Methodology

2.1. Field Sites

The study took place in the 155 km² Baker Creek Research Catchment (62°35'N, 114°25'W) (Spence & Hedstrom, 2018) located ~5 km north of the City of Yellowknife in the Northwest Territories of Canada (Figure 1).

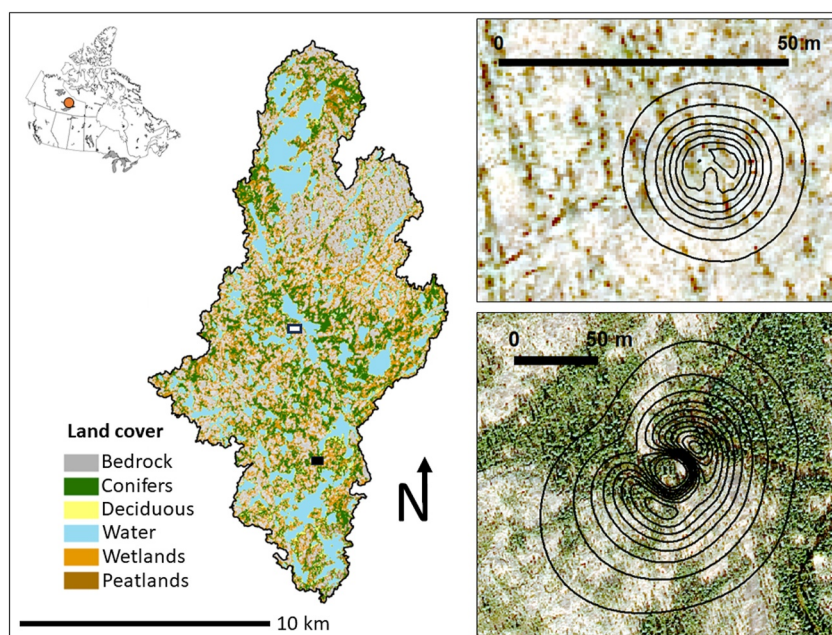


Figure 1. Maps showing flux footprints (the outermost contour contains 90% of the footprint) of each climate tower, and their locations (rectangles) within the Baker Creek Research Catchment. The white and black rectangle denote the sparse and dense canopy locations, respectively. The location of the watershed within Canada is denoted by the orange dot on the inset map. Land cover was derived using SPOT multispectral imagery classified using methods explained in Phillips et al. (2011).

The land cover in the catchment is typical of the Taiga Shield (EPA Level II Ecoregion). Exposed Precambrian Shield bedrock with sporadic stands of jack pine (*Pinus banksiana*) occupies 40% of the catchment. Soil is thin, sandy, and only occupies depressions and fracture apertures. This soil is often covered by either moss (*Polytrichum* spp.) or reindeer lichen (*Cladonia* spp.) depending on drainage conditions. Lakes and ponds cover 22% of the landscape. Wetlands and peatlands dominated by shrubs (e.g., *Alnus* and *Betula* spp.) and *Sphagnum* moss make up 16%. Lower hillslopes populated by open black spruce forests cover 22% of the catchment. These forests contain ample tamarack, and an understory of alder (*Alnus*), leatherleaf (*Chamaedaphne calyculata*), and Labrador tea (*Rhododendron groenlandicum*). Soils in these lower slopes are turbid and organic cryosols formed over sandy till and clayey glaciolacustrine deposits. The catchment is in the discontinuous permafrost zone. Permafrost is absent below exposed bedrock and lakes. Where the glaciolacustrine deposits occur, permafrost is almost always present. Active layer thickness varies among land cover types but tends to range between 0.5 and 1 m (Morse et al., 2015). The climate can be described with observations from the Meteorological Service of Canada station Yellowknife A. July has a daily average temperature of 17°C and January has a daily average temperature of −26°C. Annual unadjusted precipitation averages 290 mm, with 53% falling as solid precipitation. This area was selected for this study because Sniderhan et al. (2023) found a pattern of tree infilling across the catchment between 1972 and 2017 during which the climate warmed from an annual average of −5.2 to −4.3°C, mostly over winter. Given the dominance of black spruce in most of these dense forests, it is likely this species driving the infilling trend, though tamarack may also be a contributor. Annual unadjusted precipitation increased from 267 to 290 mm but the annual snow fraction remained steady at 53% (Environment and Climate Change Canada, 2023). Transitions from sparse forest and wetland cover to dense forest were the two most common land cover changes. Infilling of trees on bedrock ridges was less common, but still constituted a change across 4% or 5 km² of the area studied by Sniderhan et al. (2023).

2.2. Energy Partitioning

Two sites with different canopy densities were selected at which eddy covariance towers were installed (Figure 1). The sparse and dense canopy sites had tree densities of 0.04 and 0.5 m^{−2}, respectively (Table 1). The sparse canopy was dominated by jack pine (*Pinus banksiana*). The dominant species in dense forests was black spruce, although commonly found in the dense forests are individual tamarack, and occasionally jack pine and paper birch

Table 1
Specifications of the Eddy Covariance Towers Over Both the Dense and Sparse Canopies Shown in Figure 1

	Dense	Sparse
Tree density (m ⁻²)	0.5	0.04
Maximum canopy height (m)	5.5	3.8
Tower height (m)	10	4.8
Roughness height (m)	0.75	0.52
Footprint area (m ²)	18,000	6,400

Note. The area of the footprint provided includes 90% of the perceived flux.

(*Betula neoalaskana/Betula papyrifera*). Turbulent fluxes were measured for the growing season periods of May 8–24 September 2018, May 14–24 September 2019, and May 15–24 September 2020. The spring dates align with the disappearance of snow captured using trail cameras (Reconyx Hyperfire, Holmen, WI) and the autumn dates extend after senescence. Turbulent fluxes of sensible (Q_h , W m⁻²) and latent heat (Q_e , W m⁻²) above the canopy (Table 2) were measured with an eddy covariance system consisting of a three-dimensional sonic anemometer (CSAT-3, Campbell Scientific, Logan, UT) and an open-path infrared gas analyzer (LI7500, LI-COR Biosciences, Lincoln, NE) at the sparse canopy site and a krypton hygrometer (KH20, Campbell Scientific, Logan, UT) at the dense canopy site. Measurements of fluctuations in wind speed and water vapor content were taken at 10 Hz with a 30-min block averaging period. Corrections to the eddy

covariance measurements include coordinate rotation (Kaimal & Finnigan, 1994), the WPL adjustment (Webb et al., 1980), sonic path length, high frequency attenuation and sensor separation (Horst, 1997; Massman, 2000) and oxygen extinction. Using similar methods as in this study, Martínez-Cob and Suvočarev (2015) and Mauder et al. (2007) determined that both the LI-7500 and KH20 provide comparable results (Q_e) with similar uncertainty (~6 W m⁻²). Net radiation (Q^* , W m⁻²) and its components was measured at both towers with four component net radiometers (CNR4, Kipp and Zonen, Delft, The Netherlands). Ground heat flux (Q_g , W m⁻²) below the sparse canopy was calculated using a series of HOBO Tidbit temperature sensors (Onset, Bourne, MA) inserted at 10 cm intervals into a 50 cm hole drilled into the bedrock. The ground heat flux under the dense canopy was calculated using a soil temperature/moisture array located near, but outside the footprint of, the flux tower. This array contained seven soil moisture/temperature profiles located within a 100 m² area measured with Hydraprobos (Stevens, Portland, OR) at the near surface and at depths of 15, 30, and 45 cm connected to a CR1000 data logger (Campbell Scientific, Logan, UT) recording data half hourly. Hydraprobos were calibrated with soils collected around the array by inserting logger-wired sensors in soil samples placed on electronic scales while slowly adding water to saturation, and then letting the soils dry. Two wetting-drying cycles were conducted to build the calibration relationship. In 2020, the soil moisture array was not activated, and daily ground heat flux was assumed to be the average Q_g/Q^* ratio (0.03) observed in 2018 and 2019.

Table 2 summarizes the data quality at each climate tower. 2018 experienced the lowest fraction of missing data, 2019 the greatest. Energy budget closure was better at the dense stand, averaging 0.93, in contrast to 0.71 at the sparse stand. The data description below is of turbulent flux data that were adjusted for energy budget closure:

$$Q_h + Q_e = Q^* - Q_g \quad (1)$$

Table 2
Specifications on the Missing Data Fraction After Corrections Were Applied to the Turbulent Flux Estimates, and the Daily Energy Budget Closure After These Gaps Were Filled

Energy budget closure (after gap filling)		Missing data fraction	
		Q_e	Q_h
Dense canopy			
2018	0.93	0.02	0.01
2019	0.86	0.26	0.3
2020	1.02	0.09	0.1
Sparse canopy			
2018	0.67	0.09	0.11
2019	0.67	0.27	0.32
2020	0.78	0.15	0.11

Note. 2018 and 2019 include data for the entire growing season, but for the dense stand 2020 stops on July 12 with the cessation of the KH20 operation.

using methods from Charuchittipan et al. (2014). Flux footprints were estimated using methods from Kljun et al. (2015). Because the KH20 began to produce faulty measurements on 13 July 2020, after this date Q_e at the dense canopy site was calculated using the Penman-Monteith approach using methods documented in Spence et al. (2020), and Q_h calculated as the residual of the daily energy budget. Ancillary meteorological measurements to permit this calculation were taken at both towers and include air temperature (T_a , °C), relative humidity (RH, %) or vapor pressure (p , kPa) (HMP45C, Vaisala, Vantaa, Finland), wind speed (u , m s⁻¹) (013, Met One, Grants Pass, OR), and rainfall (P , mm) (TE525M, Texas Instruments, Dallas, TX). All data was logged on CR3000 loggers (Campbell Scientific).

Canopy resistance (r_c) was estimated by inverting the Penman-Monteith equation (except at the dense site after 13 July 2020). Values of r_c calculated in this fashion typically compare closely with measured stomatal resistance values over uniform vegetated surfaces (Bailey & Davies, 1981). Over sparse sites (i.e., understory dominated by lichen and moss) r_c becomes less of a diagnostic metric of stomatal resistance, but rather the general surface resistance to water efflux. Because of this, r_c can become artificially high

(Kasurinen et al., 2014), and therefore additional metrics were used to further assess the conditions that control evapotranspiration. Because it quantifies trade-offs between the predominance of radiation versus aerodynamic influences as canopy density changes, a good metric for assessing controlling factors is the Jarvis and McNaughton (1986) decoupling term, Ω :

$$\Omega = \frac{\frac{\Delta}{\gamma} + 1}{\frac{\Delta}{\gamma} + 1 + \left(r_c/r_a\right)} \quad (2)$$

where Δ is the slope of the saturation vapor pressure-temperature curve ($\text{kPa } ^\circ\text{C}^{-1}$), γ is the psychrometric constant ($\text{kPa } ^\circ\text{C}^{-1}$), r_c is canopy resistance (s m^{-1}) and r_a is aerodynamic resistance (s m^{-1}). Aerodynamic resistance was calculated using wind measurements as described in Oke (1987). Ω ranges from zero to one, and when forests are sparser and more aerodynamically rough, r_a is lower than r_c and Ω would be expected to shrink. To support analysis of Ω values, Priestley and Taylor's (1972) α was calculated, as was the rate at which latent heat fluxes change relative to changes in equilibrium, $Q_e(\text{eq})$ and imposed, $Q_e(\text{aero})$, evaporation, using methods summarized in Iida et al. (2009).

$$Q_e(\text{eq}) = \frac{\Delta}{\Delta + \gamma} \cdot (Q^* - Q_g) \quad (3)$$

$$Q_e(\text{aero}) = \frac{\rho \cdot c_p \cdot \text{VPD} \cdot g_a}{1 + \left(g_a/g_c\right)} \quad (4)$$

where ρ is the air density (kg m^{-3}), c_p is the specific heat of air (J kg^{-1}), VPD is the vapor pressure deficit (kPa), g_a is aerodynamic conductance (m s^{-1}) and g_c is canopy conductance (m s^{-1}). The latter two are the inverse of aerodynamic and canopy resistance noted above.

2.3. Vegetation Water Use and Soil Water State

Over and understory vegetation species and soils were sampled for stable isotopes of hydrogen and oxygen during the growing seasons of 2018, 2019, and 2020 prior to leaf-out through senescence (May through September) following methods described in McCutcheon et al. (2017). Vegetation and soil sample total numbers are 510 and 223, respectively. Xylem water samples were taken from the overstory species of tamarack, jack pine and black spruce and understory species of alder, leatherleaf, and Labrador tea. Stems were sampled by clipping segments from thin branches which were then cut into 5 mm segments and placed in cryogenic vials with the bark intact. Soils were sampled at the same time as vegetation at 10 cm intervals to the depth of the frost table which descended to ~ 50 cm below the ground surface each summer but sometimes reached as deep as 100 cm. Soils were collected from pits dug with trowels to the desired depths. Soil samples were placed in freezer bags and double bagged. Logistical challenges limited access to the sample sites within the flux tower locations to periods in June and September each year. To augment these samples, vegetation and soil sampling every 2 weeks also occurred at road accessible sites comparable in topographic position and canopy density as the tower footprints.

There is a long history of sampling water for stable isotope analysis in the Baker Creek Research Catchment (Gibson & Reid, 2010; Gibson et al., 1998; Spence et al., 2014). From these studies there exists a ~ 25 -year record of samples collected prior to the 2018–2020 growing seasons that were used to provide context for the soil and vegetation samples described above. Prior to and during this study, rain was sampled from Type B precipitation gauges lined with oil to prevent evaporation or from Nalgene bottles connected to a funnel via long length plastic tubing to prevent evaporation (Gröning et al., 2012). Bulk snow samples were collected in Ziploc bags, allowed to melt and the water collected in either 30 ml polyethylene bottles or 5 ml glass bottles. Any runoff samples were collected in 30 ml polyethylene bottles minimizing headspace and sealed lids to minimize potential for evaporation.

Soil samples were stored in freezer bags for no more than 3 weeks. The soil water was analyzed using direct vapor equilibration methods outlined in Wassenaar et al. (2008) and Hendry et al. (2015). The plant water was cryogenically extracted using methods described in Koeniger et al. (2011) and then analyzed using isotope ratio mass

spectrometry. All stable isotope values are reported as parts per thousand (δ or per mil (‰)) according to the Vienna Standard Mean Ocean Water-Standard Light Antarctic Precipitation (VSMOW-SLAP) scales. Sample analysis took place at the University of Saskatchewan using Los Gatos Research (ABB Group, Zurich, Switzerland) liquid water Off-Axis Integrated-Cavity Output Spectroscopy (Off-Axis ICOS) with an accuracy of $\pm 1.0\text{‰}$ for $^2\text{H}/\text{H}$ and $\pm 0.2\text{‰}$ for $^{18}\text{O}/^{16}\text{O}$, or an Elementar Isoprime isotope ratio mass spectrometer (IRMS). Hydrogen isotopic compositions of water were determined by reduction of water to hydrogen by reaction elemental chromium following the method of Morrison et al. (2001). Briefly, $0.8 \pm \mu\text{L}$ of water was injected into a quartz reactor containing elemental chromium at 1050°C . The resultant H_2 gas was separated on a 1 m mol sieve gas chromatography column. To minimize memory effects, two replicates of each sample were injected, and the first measurement discarded. Resultant raw δ values of the measured hydrogen were normalized to the SMOW-SLAP scale by analyses of two calibrated waters. For oxygen isotopes, the $\text{CO}_2\text{-H}_2\text{O}$ equilibration technique of Epstein and Mayeda (1953) was used. A micromass multiframe device connected to an Elementar Isoprime IRMS at 25°C was used for all $\text{CO}_2\text{-H}_2\text{O}$ equilibrations. Results are reported relative to the VSMOW-SLAP scale by normalizing to in-house lab standards. These standards for both the laser and mass spectrometers were CSNOW: -202.6‰ ^2H and -26.51‰ ^{18}O and LVIC: 9.7, 0.57, and -0.1‰ for ^2H , ^{18}O and ^{17}O .

Analysis of the stable isotope values began by drafting dual isotope plots as suggested by McDonnell (2014) to disentangle ages and origins of water in both soils and vegetation. A local meteoric water line (LMWL) has been calculated for the Yellowknife region (Gibson & Reid, 2010; Gibson et al., 1998), and was updated using values obtained as part of this sampling campaign using the form:

$$\delta^2\text{H} = a \cdot \delta^{18}\text{O} + b \quad (5)$$

Local evaporative lines for each soil depth and plant species were similarly derived as their slopes are indicative of evaporative enrichment (McCutcheon et al., 2017). Line conditioned excess values indicative of fractionation during evaporation were calculated following:

$$\text{lc-excess} = \delta^2\text{H} - a \cdot \delta^{18}\text{O} - b \quad (6)$$

Lc-excess values were calculated for each 10 cm soil depth and each vegetation species as these values denote departure from meteoric water lines and, in turn, are indicative of the age of water. Lower more negative lc-excess values imply water has had more opportunity to be exposed to evaporative enrichment and has spent more time in the soil and/or vegetation (Landwehr & Coplen, 2006; Sprenger, Tetzlaff, Buttle, Laudon, & Soulsby, 2018). Kruskal Wallis tests conducted in the *R* computing environment (Version 3.5.1; Hollander & Wolfe, 1973) were applied to all the samples from every year to determine if stable isotope values in precipitation were different from those in soils and if soils were different again from the water in plants. As well, these tests were used to determine if lc-excess values of soils and vegetation for each year were significantly different than 0 (Tetzlaff et al., 2021). There can be memory from cumulative evapotranspiration and precipitation left in soil and plant water signatures that indicate the temporal scale of fluxes that most influence water state (i.e., volume and age) (Sprenger, Tetzlaff, Buttle, Carey, et al., 2018). To determine this scale, time series of lc-excess versus 7-, 14- and 30-day evapotranspiration (measured using the Q_e measurements described above) and rainfall totals were evaluated using linear regression as well as with breakpoint identification in piecewise linear regression using the *segmented* package in the *R* computing environment (Version 3.5.1; Muggeo, 2008) to determine the presence of a relationship. The non-linear relationship was considered better than the linear relationship if it met two conditions; a higher r^2 value, and the percent difference between the slopes before and after the breakpoint was greater than 10%.

3. Results

3.1. Meteorological Conditions

Average May–September air temperature (1991–2020) reported at the Environment and Climate Change Canada meteorological station Yellowknife A is $11.7 \pm 4.8^\circ\text{C}$ (Environment and Climate Change Canada, 2023). At Yellowknife, 2018 to 2020 were cooler, but still normal, years at 10.4°C , 10.2°C and 10.8°C , respectively. Leaf expansion began in 2018 between May 31 and June 2, and between June 9 and 13 in 2019. The camera used to document snow disappearance and leaf expansion of the trees stopped working 7 June 2020, but leaf expansion is

Table 3
Average of Growing Season Daily (Approximately Mid May to End of September) Net Radiation (Q^*), Sensible Heat (Q_h), and Latent Heat (Q_e); Gap Filled and Energy Budget Closed

	Year	Sparse	Dense
Q_e ($W m^{-2}$)	2018	29	36
	2019	24	36
	2020	27	39
Q_h ($W m^{-2}$)	2018	79	62
	2019	83	61
	2020	85	61
Q^* ($W m^{-2}$)	2018	106	102
	2019	103	99
	2020	109	101
β	2018	2.72	1.72
	2019	3.45	1.69
	2020	3.15	1.56
Q_e/Q^*	2018	0.27	0.35
	2019	0.23	0.36
	2020	0.25	0.38
ET (mm)	2018	142	177
	2019	114	172
	2020	126	182
P (mm)	2018	244	274
	2019	102	136
	2020	186	197
ET/P	2018	0.58	0.64
	2019	1.1	1.26
	2020	0.68	0.92
VPD (kPa)	2018	0.56	0.5
	2019	0.57	0.52
	2020	0.59	0.52
T_a ($^{\circ}C$)	2018	11.6	11.3
	2019	11.9	11.7
	2020	12.4	12.1
r_c ($s m^{-1}$)	2018	611	250
	2019	589	348
	2020	541	318
r_a ($s m^{-1}$)	2018	9.1	17.5
	2019	9.5	18.2
	2020	9.0	15.6
Ω	2018	0.07	0.2
	2019	0.06	0.08
	2020	0.05	0.14
$Q_e/Q_e(eq) = (\alpha)$	2018	0.44	0.56
	2019	0.49	0.51
	2020	0.55	0.77

expected to be similar to 2019 as snow disappeared within a day in both years. The 2004–2020 average basin scale spring snow water equivalent documented with the Baker Creek snow course network is 79 mm (Spence & Hedstrom, 2018). Basin scale spring snow water equivalent in 2018, 2019 and 2020 was 65, 65 and 85 mm, respectively. Average growing season (May–September) precipitation at Yellowknife A (1991–2020) is 162 ± 51 mm. At Yellowknife, all three growing seasons were wetter than average. 2018 experienced 256 mm of precipitation with June 2018 being the wettest in 50 years, receiving 114 mm of precipitation relative to the average of 29 mm. 2019 and 2020 were drier, but above normal with 192 and 223 mm, respectively. The convective nature of summer precipitation in this region can result in high spatial variation in rainfall, so these values are provided for context, recognizing that precipitation at the dense and sparse stands presented below were different (Table 3; Figure 2) and that 2019 was relatively drier than 2018 and 2020.

3.2. Energy Partitioning

Air temperatures at the two stands were very similar with seasonal averages within $0.3^{\circ}C$, with the sparse canopy slightly warmer across all 3 years. This applies to the VPD as well, with the sparse canopy drier by less than 0.1 kPa (Table 3). This is within the accuracy of the thermohygrometers, so air temperatures and vapor pressures at the two sites can essentially be considered the same. Net radiation rose steadily from the beginning of the growing season to its peak each year in the second half of June (day ~ 165 –180) after which it steadily declined (Figure 3). Sensible heat dominated turbulent fluxes, particularly over the sparse canopy (Figure 3; Table 3), where the Bowen ratio averaged 3.1 over the 3 years. In the dense canopy, this value averaged 1.7. While Q_e was a smaller portion of the two turbulent fluxes, evapotranspiration dominated the growing season water budget. The ratio of evapotranspiration (ET) to rainfall (P) was always high, averaging 0.79 and 0.94 in the sparse and dense canopies, respectively. This was especially so during the drier 2019 season when ET exceeded P. Growing season ET at the sparse stand averaged 127 mm, and 177 mm from the dense stand. There were always lower seasonal rates of ET from the sparse canopy. Evapotranspiration rates from the two canopies were most similar during the wet conditions of 2018 (Table 3). Seasonal differences in Q_e are larger than those documented by studies comparing KH20 and LI7500 instruments (Martínez-Cob & Suvočarev, 2015; Mauder et al., 2007), so these differences are not due to the different sensors.

Aerodynamic resistance was higher (3-year average of $17 \pm 1.3 s m^{-1}$ vs. $9.2 \pm 0.3 s m^{-1}$) over the dense stand because of the smoother canopy (Figure 4; Table 3), and possibly because of lower wind speeds (Figure 3). The sparse stand exhibited high r_c of $590 \pm 35 s m^{-1}$ over the three years but r_c was lower and less consistent over the dense stand at $305 \pm 50 s m^{-1}$. Canopy resistance was highest during drier periods, (e.g., late July 2018; days 200–212) (Figure 4). Values of α were well below 1.26 in these two stand types and values were negatively related to r_c (Table 3), particularly in the sparse stand. Values above 1.26 did occur when r_c was less than $175 s m^{-1}$ at the dense stand and $243 s m^{-1}$ at the sparse stand. Small values of Ω from both stands indicate strong canopy control of ET (Table 3). A change in behavior becomes apparent when the canopies become wet. Latent heat fluxes spike, r_c decreases and Ω increases (e.g., 1 July 2019; day 182). While present in both

Table 3
Continued

	Year	Sparse	Dense
$Q_e - \Omega * Q_e(\text{eq})$ slope	2018	0.25	0.29
	2019	0.17	0.10
	2020	0.15	0.21
$Q_e - 1 - \Omega * Q_e(\text{aero})$ slope	2018	0.07	0.06
	2019	0.05	0.05
	2020	0.05	0.04

Note. Dense canopy Q^* data gaps were estimated using a relationship between $K\downarrow$ and Q^* ($K\downarrow * 0.7 - 35.7 = Q^*$) derived with daily data from 2018. Fluxes, Bowen ratio (β), water budget (rainfall, P ; evapotranspiration, ET), and meteorological (vapor pressure deficit, VPD; air temperature, T_a) data are for the whole season of 2020, but aerodynamic resistance (r_a), surface resistance (r_c) and Ω data from the dense canopy ceased on July 12.

stands, this behavior is more pronounced over the dense stand, particularly in 2019 (Figure 4). When a canopy is wet, canopy VPD becomes negligible and Ω increases. Under these conditions, ET is controlled by Q^* and not the dryness of the atmosphere, and ET becomes independent of vegetation control over resistance. Latent heat fluxes were not very responsive to VPD and r_c . Rather, Q_e in both canopies was more responsive to temperature and Q^* . This is indicated by slopes between Q_e and $\Omega * Q_e(\text{eq})$ (Table 3; Figure 5) that average 0.19 in the sparse stand and 0.2 in the dense stand which are an order of magnitude higher than those between Q_e and $1 - \Omega * Q_e(\text{aero})$. The $Q_e - \Omega * Q_e(\text{eq})$ slopes were higher during the two wetter years in the dense canopy (Table 3; Figure 5). Typically, higher Q_e was controlled by radiation, particularly in the dense stand. This is indicated by the higher Ω (0.13 vs. 0.05), lower r_c (372 vs. 598 s m^{-1}) and higher $Q_e/Q_e(\text{eq})$ (0.61 vs. 0.5) in the dense canopy relative to the sparse. The slightly higher slope of the $Q_e - \Omega * Q_e(\text{eq})$ curve in the denser forest (0.27 vs. 0.18) indicates a more freely evaporating canopy with increased density.

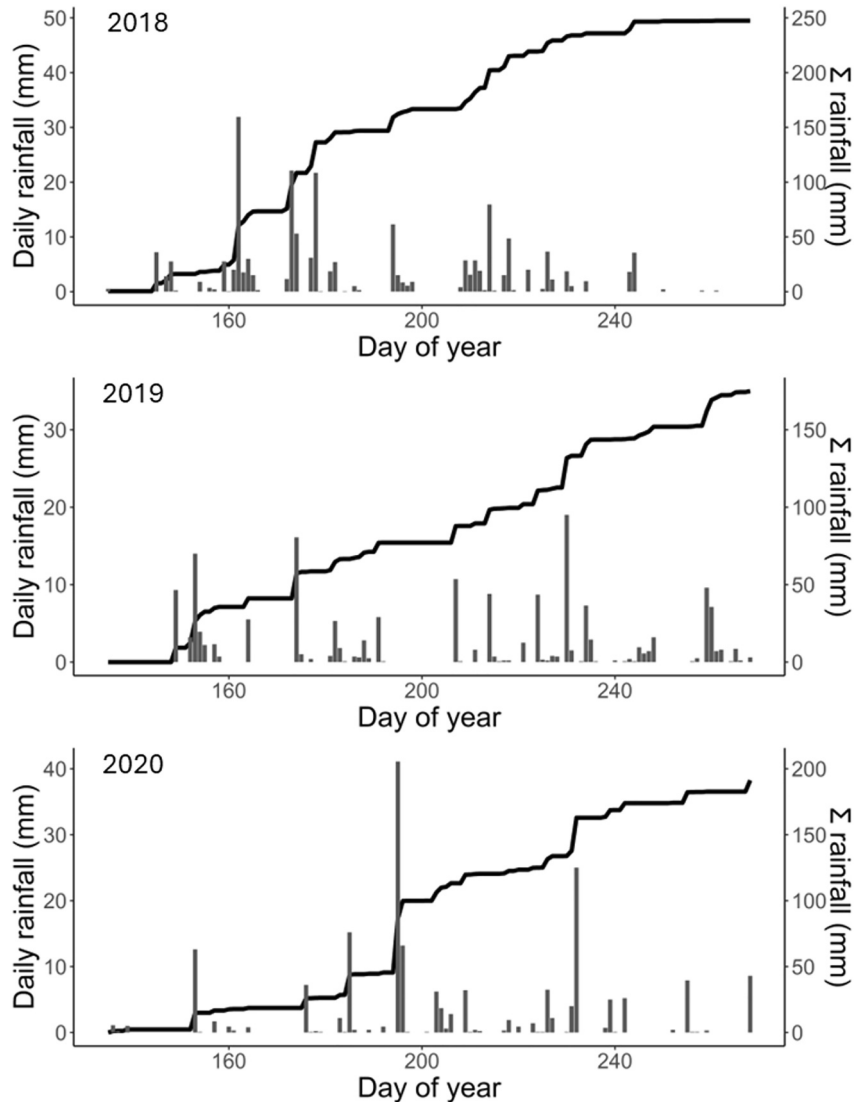


Figure 2. Daily rainfall rates and cumulative growing season rainfall for each of the study years over the dense canopy site.

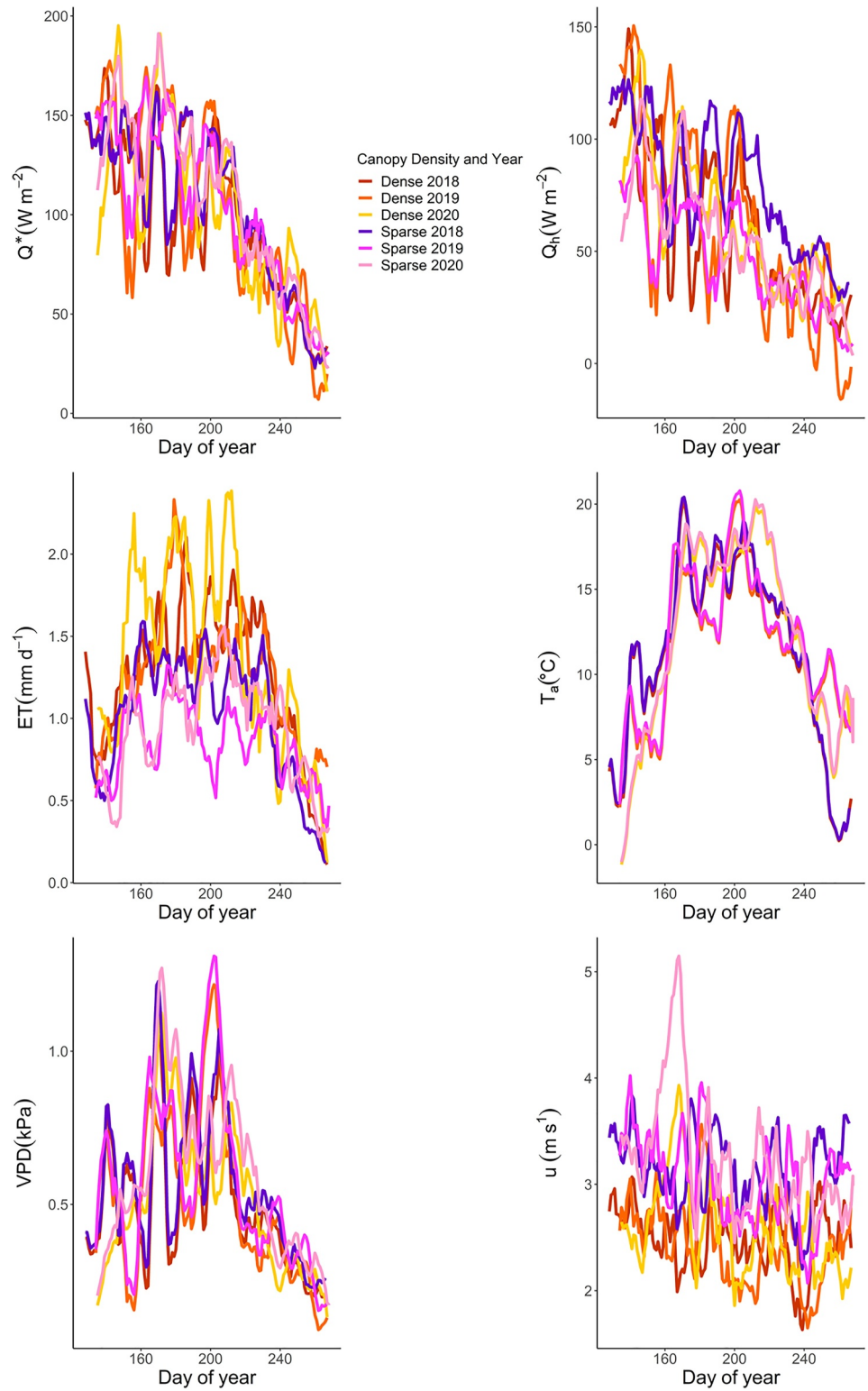


Figure 3. Seven-day running means of net radiation (Q^*), sensible heat (Q_h), evapotranspiration (ET), air temperature (T_a), vapor pressure deficit (VPD), and wind speed (u) over each canopy over the three study years.

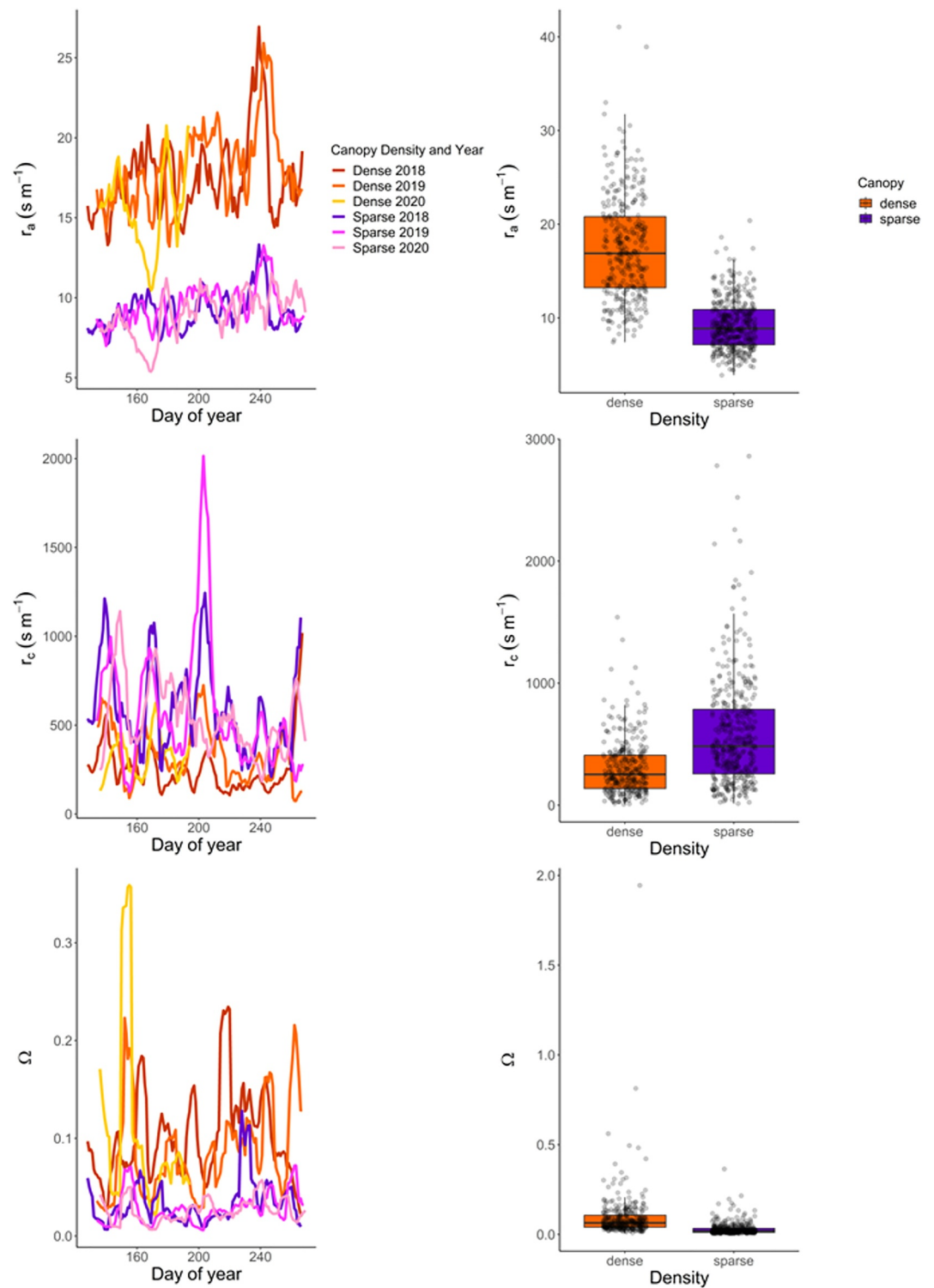


Figure 4. Seven-day running means of aerodynamic resistance, canopy resistance and Ω over each canopy for the three study years. Boxplots of daily values are presented on the right showing a box with 3-year mean and \pm one standard deviation with whiskers of the 25% and 75% percentiles.

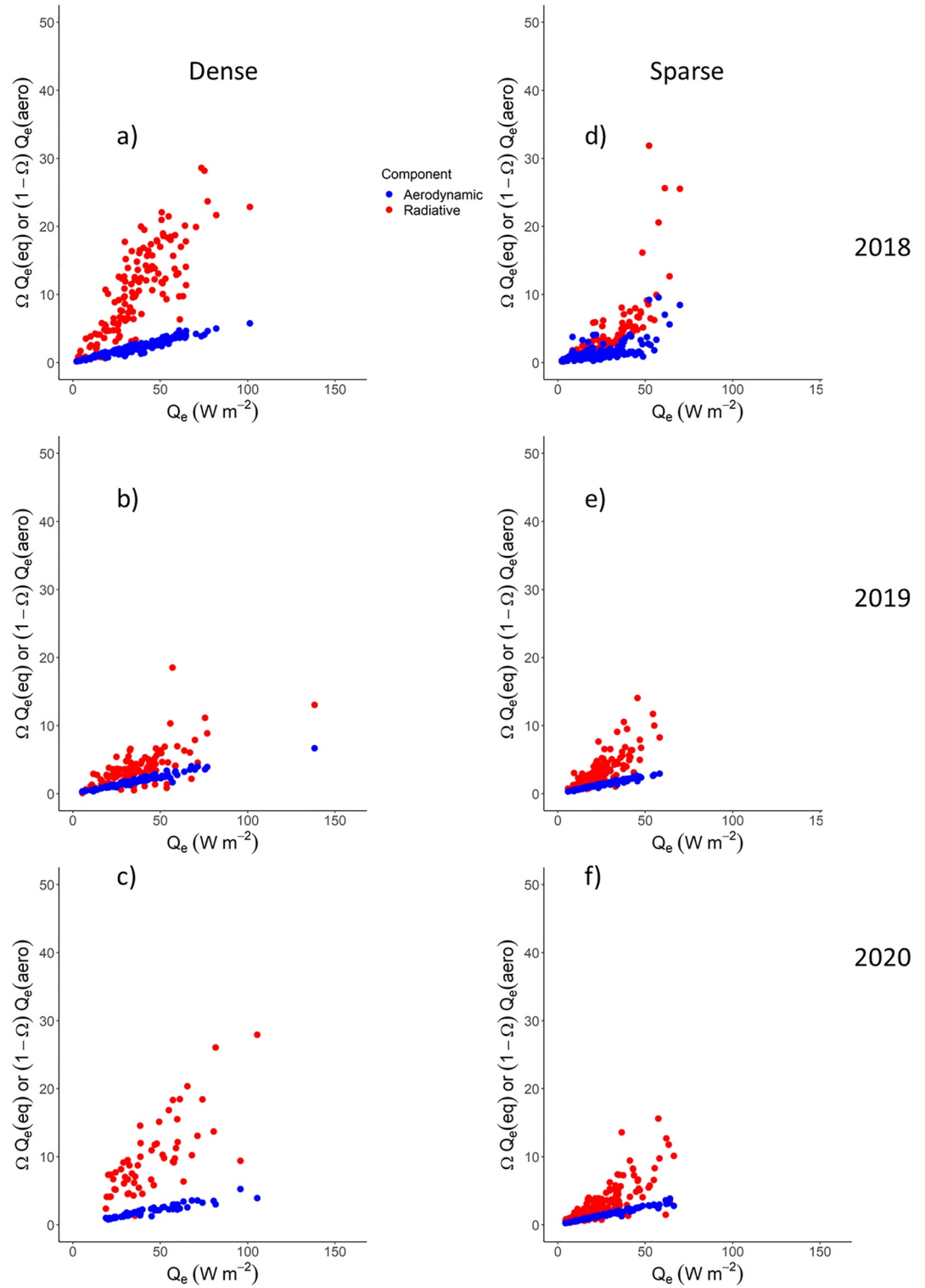


Figure 5. (a–c) Sensitivity of latent heat flux to aerodynamic and radiative forcings for the dense, and (d–f) the sparse canopies from (a, d) 2018, (b, e) 2019, and (c, f) 2020.

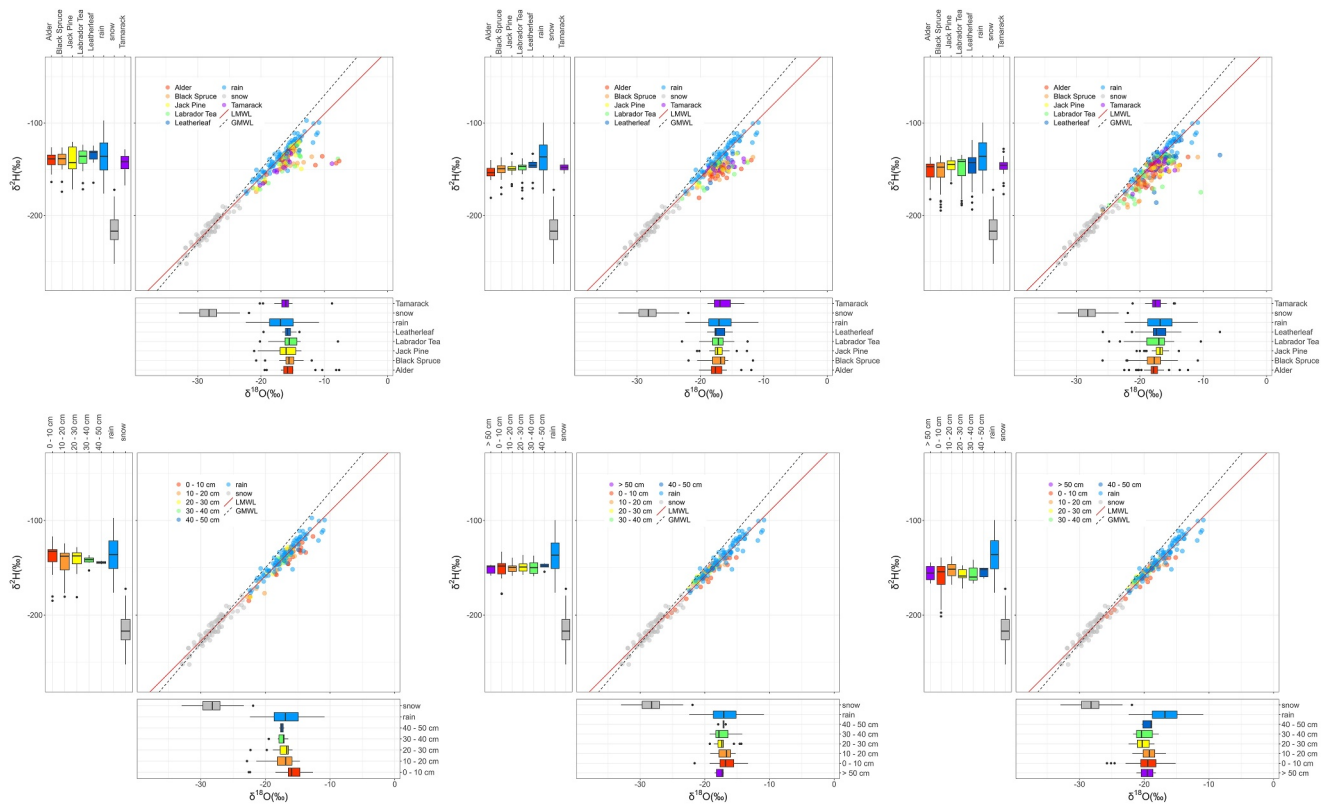


Figure 6. (top) Dual isotope plots of vegetation species and (bottom) soil depths by year (2018–2020, left to right). Boxplots show mean, standard deviations and range of stable isotope values by species and soil depth and precipitation phase. The local meteoric water line (LMWL) described in Equation 6 is illustrated to show the slope relative to the Global Meteoric Water Line. The LMWL is represented by $\delta^2\text{H} = 6.86 \cdot \delta^{18}\text{O} - 21.59$.

3.3. Vegetation Water Use

Applying the new precipitation isotope results collected during this study updates the LMWL of Gibson and Reid (2010):

$$\delta^2\text{H} = 6.7 \cdot \delta^{18}\text{O} - 23.2 \quad (7)$$

to:

$$\delta^2\text{H} = 6.86 \cdot \delta^{18}\text{O} - 21.59 \quad (8)$$

There is clear separation in isotopic signatures between rain and snow, with average $\delta^{18}\text{O}$ values of -16.9‰ and -28.2‰ , respectively (Figure 6). While there was some seasonality in the stem water isotopic signatures, each species tended to emulate rain, rather than snow (Figure 6). While isotopic signatures did not differ among the plant species, the pattern of tree water use differed among the three study years. Early in the 2018 growing season, plants tended to use water that resembled snowmelt (low values of $\delta^2\text{H}$ between -135 and -175‰) (Figure 7). As the summer progressed, values of $\delta^2\text{H}$ in plant water became more representative of rainfall, which was more enriched in $\delta^2\text{H}$ and $\delta^{18}\text{O}$ relative to snowfall. June 2018 was very wet and coincided with higher, less negative lc-excess values in stem water of all species, indicating less evaporative fractionation within plant water sources. However, from July onwards, with less rainfall, values of lc-excess in all species became more negative, particularly in alder, indicating more evaporatively enriched plant water sources. The pattern in the drier 2019 growing season was similar, though early season stem water was generally more evaporatively enriched (more negative lc-excess values) than in 2018 (Figure 7; Table 4). Additionally, stem water values of $\delta^2\text{H}$ and lc-excess increased and became less negative near the end of the 2019 season, unlike 2018. At the beginning of the 2020 growing season (the year of the highest snow water equivalent), stem water resembled snowmelt, as in 2018. The

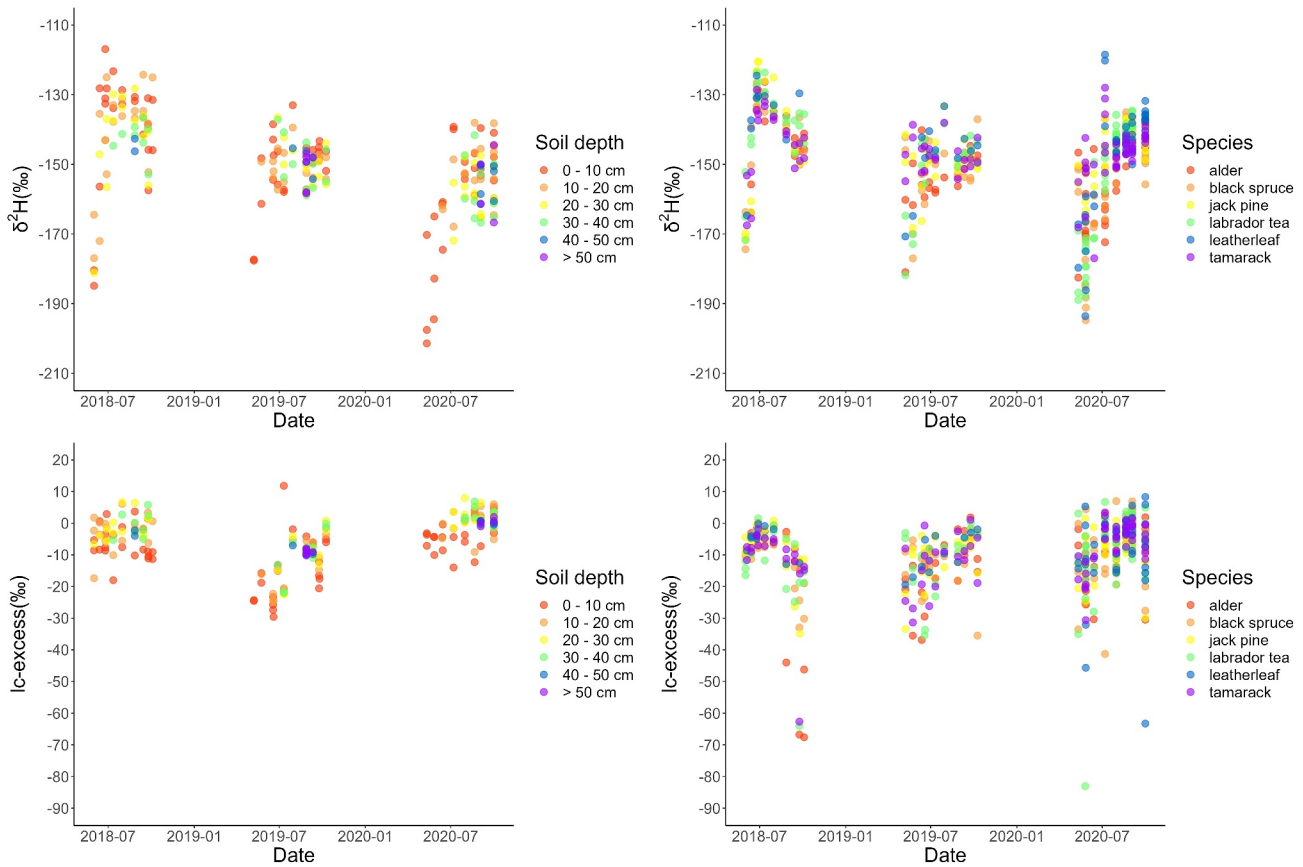


Figure 7. Vegetation (right column) and soil (left column) $\delta^2\text{H}$ and lc-excess bi-weekly values through the 3 years of the study period.

2020 growing season continued the pattern of plants using water enriched in $\delta^2\text{H}$ and $\delta^{18}\text{O}$ from rainfall in the middle of the summer, as indicated by higher average lc-excess values, representative of heavier, less evaporatively enriched rainfall (Table 4; Figure 7). There were no statistically significant relationships found between 7-, 14-, and 30-day evapotranspiration and lc-excess values. There are statistically significant non-linear relationships between 7-, 14-, and 30-day rainfall and lc-excess among plants (Figure 8; Table 5), that better fit the

Table 4
Annual Averages and Standard Deviations of $\delta^{18}\text{O}$, $\delta^2\text{H}$, and Lc-Excess Values for Each Year by Plant Species

Year	All species	Black spruce	Jack pine	Tamarack	Alder	Labrador tea	Leatherleaf
lc-excess							
2018	-11 ± 12	-12 ± 8.3	-8.5 ± 8.6	-11 ± 13	-16 ± 23	-12 ± 13	-5.5 ± 4.5
2019	-9.0 ± 11	-12 ± 7.7	-11 ± 7.6	-13 ± 9.2	-15 ± 10	-12 ± 9.8	-10 ± 6.2
2020	-9.2 ± 10	-8.4 ± 9.8	-8.0 ± 6.9	-6.5 ± 7.4	-7.9 ± 8.6	-7.9 ± 12	-8.6 ± 14
$\delta^{18}\text{O}$							
2018	-17 ± 2.6	-16 ± 1.8	-16 ± 2.4	-16 ± 2.2	-15 ± 3.3	-15 ± 2.3	-16 ± 1.5
2019	-17 ± 2.2	-17 ± 2.0	-17 ± 1.7	-16 ± 1.7	-17 ± 1.8	-17 ± 2.2	-17 ± 1.3
2020	-17 ± 2.0	-18 ± 2.3	-17 ± 1.2	-17 ± 1.2	-18 ± 1.8	-18 ± 2.4	-17 ± 2.7
$\delta^2\text{H}$							
2018	-152 ± 14	-140 ± 11	-142 ± 17	-144 ± 10	-140 ± 9.6	-139 ± 12	-136 ± 11
2019	-147 ± 12	-151 ± 8.9	-150 ± 7.4	-147 ± 4.6	-154 ± 8.2	-151 ± 11	-148 ± 11
2020	-147 ± 12	-152 ± 15	-146 ± 7.0	-147 ± 8.6	-152 ± 11	-150 ± 17	-148 ± 16

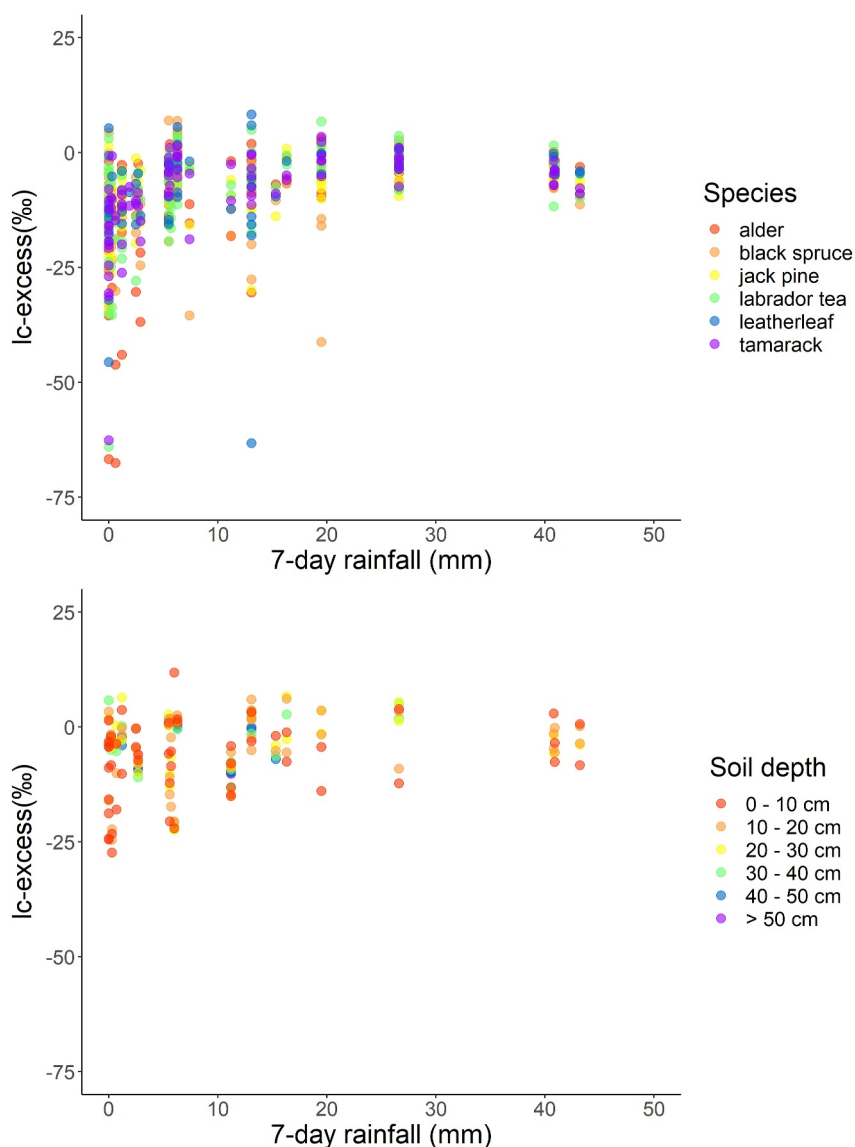


Figure 8. Lc-excess versus 7-day rainfall for vegetation species (top) and soil depths (bottom).

Table 5
Results of Linear and Piecewise Linear Regression of Rainfall and Vegetation Lc-Excess for the Period of Study

Period	Linear		Piecewise		s_1	s_2
	r^2	p	r^2	Breakpoint (mm)		
7-day	0.11	<0.001	0.22	6	1.8	-1.8
14-day	0.13	<0.001	0.21	14	0.9	-0.9
30-day	0.13	<0.001	0.18	33	0.38	-0.35

Note. s_1 and s_2 denote slopes before and after the breakpoint and are used to assess fit relative to linear regression. All results are significant with 90% confidence.

data than the linear relationships. The degree of evaporative enrichment indicated in the Lc-excess values in soil and vegetation when 7-, 14-, and 30-day rainfall is less than 6, 14, and 33 mm, respectively, indicates both over and understory plant species access older water during these sustained dry conditions and younger recently precipitated water when it is wetter.

3.4. Soil Water State

Isotope values in soil columns under both dense and sparse canopies are more comparable to rain rather than snow (Figure 6) except for a few select samples from shallow soils. Kruskal Wallis rank sum tests indicate that precipitation, soil, and vegetation $\delta^{18}\text{O}$ values were not identical ($\chi^2 = 189.26$, $p = 2.2 \times 10^{-16}$) with soils relatively less depleted in heavier isotopes than plants (Tables 4 and 6). Average $\delta^{18}\text{O}$ and $\delta^2\text{H}$ values of soils at depth (i.e., >40 cm) trend toward those values of snow but remain clearly influenced by a

Table 6
Annual Averages and Standard Deviations of $\delta^{18}\text{O}$, $\delta^2\text{H}$, and Lc-Excess Values for Each Year by Soil Depth

Year	All depths	0–10 cm	10–20 cm	20–30 cm	30–40 cm	40–50 m	>50 cm
Lc-excess							
2018	-3.2 ± 5.1	-6.1 ± 5.3	-2.5 ± 5.0	-1.2 ± 4.1	-0.5 ± 4.0	-3.1 ± 1.2	n/a
2019	-11 ± 7.8	-14 ± 10	-13 ± 7.4	-10 ± 6.8	-9.8 ± 7.0	-9.1 ± 1.2	-9.0 ± 0.8
2020	0.1 ± 4.3	-3.4 ± 5.1	1.1 ± 3.8	2.6 ± 2.5	2.1 ± 2.5	0.3 ± 0.5	1.4 ± 1.2
$\delta^{18}\text{O}$							
2018	-17 ± 2.1	-18 ± 3.0	-16 ± 1.0	-17 ± 0.8	-18 ± 1.6	-16 ± 0.9	n/a
2019	-17 ± 1.5	-16 ± 1.9	-17 ± 1.3	-18 ± 0.6	-17 ± 1.0	-17 ± 1.1	-19 ± 0.6
2020	-20 ± 1.9	-20 ± 2.6	-19 ± 1.6	-20 ± 1.3	-19 ± 1.3	-20 ± 1.1	-20 ± 1.4
$\delta^2\text{H}$							
2018	-142 ± 15	-150 ± 22	-134 ± 4.5	-138 ± 5.6	-147 ± 9.1	-135 ± 15	n/a
2019	-150 ± 7.3	-151 ± 11	-148 ± 7.0	-151 ± 4.7	-150 ± 4.0	-149 ± 4.2	-150 ± 5.2
2020	-156 ± 12	-164 ± 17	-153 ± 7.9	-155 ± 7.7	-150 ± 7.5	-157 ± 6.0	-155 ± 10

rainfall signature (Table 6 and Figure 6). Kruskal Wallis rank sum tests demonstrate isotopic signatures of soil water under dense and sparse canopies were not identical ($\chi^2 = 5.3557, p = 0.02$). From the middle of the growing season onwards, soil water at the dense site tended toward more negative Lc-excess than the sparse site. This is illustrated by Lc-excess patterns in soil columns under sparse and dense canopies in 2020 after day of year 250 (Figure 9).

Each year exhibited very different patterns of $\delta^2\text{H}$ and Lc-excess in the soil columns (Figures 7 and 10). In wet 2018, soil Lc-excess values remained near -4% and $\delta^2\text{H}$ signatures emulated that of snow to the frost table ($\sim 180\%$) immediately following leaf expansion. Ample rain during June (days 152–181) increased Lc-excess values closer to 0 and $\delta^2\text{H}$ values migrated to $\sim -135\%$, particularly near the soil surface (Figures 7 and 10). At the beginning of July, drier conditions led to more negative Lc-excess and evaporatively enriched water in shallow soil depths. This continued into July when conditions were drier and shallow soil water was evaporatively enriched (\sim days 182–200). These more negative Lc-excess values appeared in deeper soils by the end of July (\sim day 212), while lower less negative Lc-excess values occupied shallower depths. Rainfall events after \sim day 212 added rainfall enriched in $\delta^2\text{H}$ ($\sim -135\%$) which was followed by evapotranspiration that resulted in more negative Lc-excess within the soil column around day 257 (Figures 7 and 10). By the end of the growing season in 2018, the Lc-excess values were more uniform near 0 throughout the soil column. The dry conditions in 2019 resulted in different Lc-excess signatures in the soil profile, as there were uniform more negative Lc-excess values until late July (\sim day 205) (Figure 10). This implies the soil water that remained at the end of the 2018 season in addition to any 2019 snowmelt infiltration was subject to evaporative enrichment well into 2019. This mixture is reflected in the isotopic composition with $\delta^2\text{H}$ values averaging -151% in May and June. $\delta^2\text{H}$ increased through July and August (days 182–243) in response to rain corresponding to higher soil moisture near the surface (Figure 11). However, by the end of the growing season (September, \sim day 244) the soil had started to dry and Lc-excess values were becoming more negative, indicative of evaporative enrichment (Figures 10 and 11). As in 2019, the 2020 growing season began with higher less negative Lc-excess values and less enriched $\delta^2\text{H}$ values indicative of younger water shallow in the soil column. Like 2018, Lc-excess values initially became more negative at the

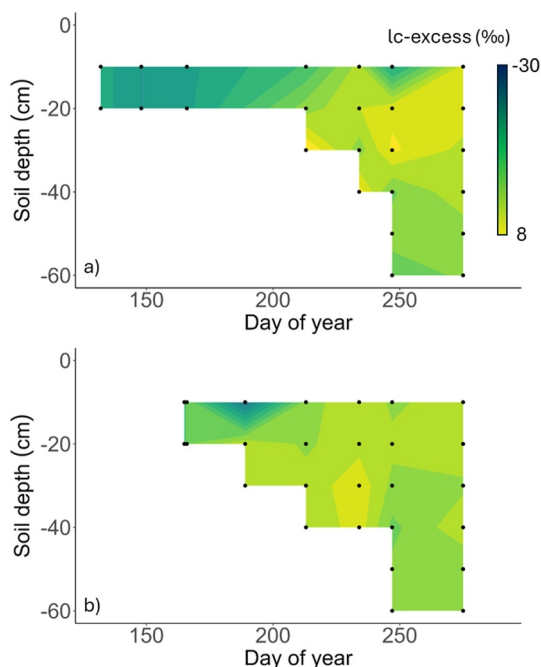


Figure 9. Soil isotopic states in 2020; Lc-excess (%) under sparse (top) and dense (bottom) canopies during the 2020 growing season. The black dots denote sampling days and depths. The absence of data below the contour plots implies the presence of frozen ground and the lower edge of the plots approximates the frost table depth as soils were sampled only down to the frost table.

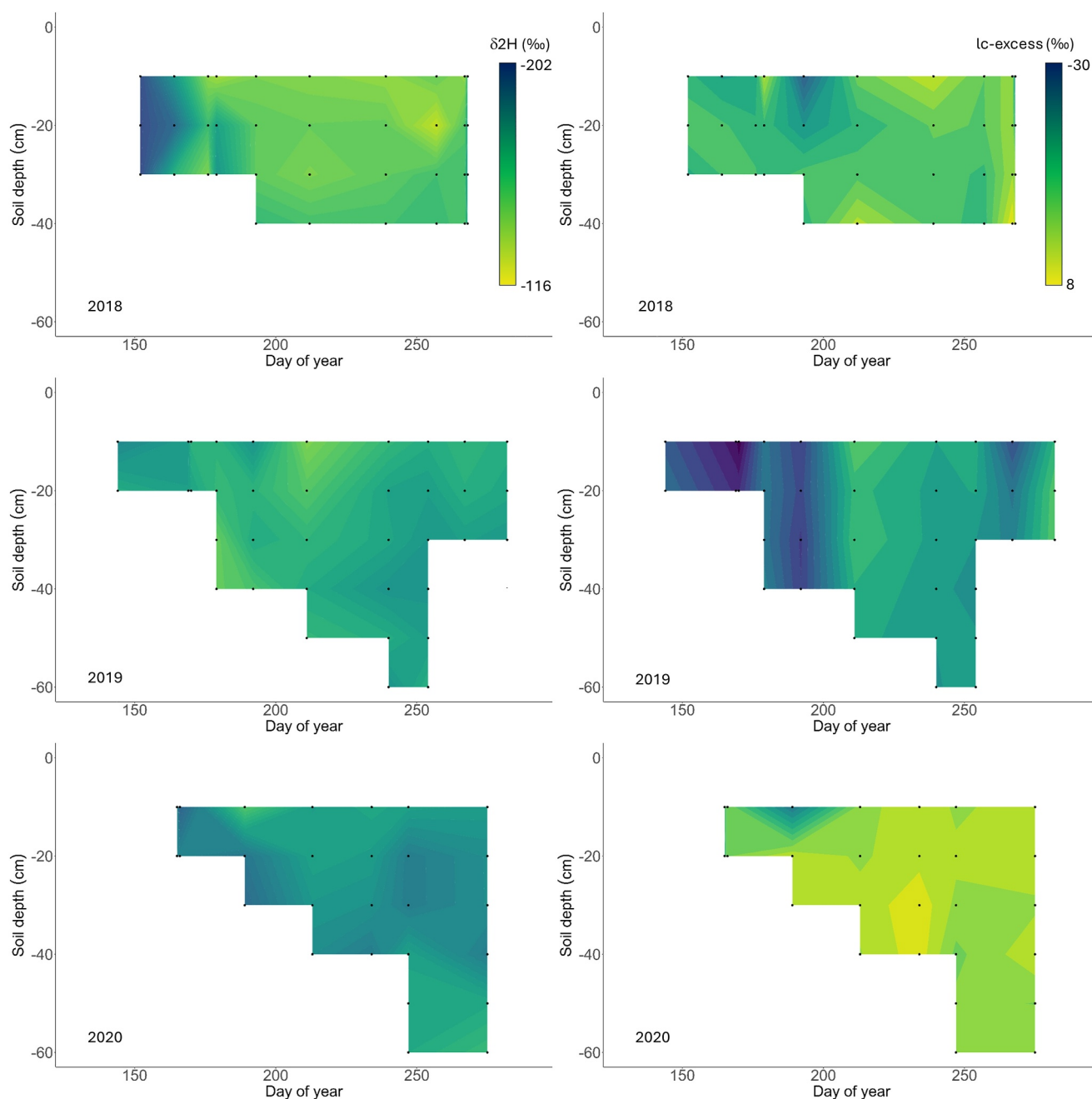


Figure 10. Soil isotopic states among all three study years; $\delta^2\text{H}$ (left) and lc-excess (right) (‰) in the 2018, 2019 and 2020 growing seasons (top to bottom) in soils under the dense canopy. The black dots denote sampling days and depths. As with Figure 9, the absence of data below the contour plots implies the presence of frozen ground and the lower edge of the plots approximates the frost table depth as soils were sampled only down to the frost table.

beginning of the growing season and then increased as new rain consistently entered the soil column. This is reflected in $\delta^2\text{H}$ values that varied little from July to September ($-152.5 \pm 0.98\text{‰}$) (Figures 7 and 10).

4. Discussion

4.1. Energy Partitioning

Both sparse and dense canopies exhibited comparable Q^* . Estimates of Q_e/Q^* were 0.25 and 0.36 over the sparse and dense canopies, respectively, which are within the range of that documented across the Canadian taiga (Eaton

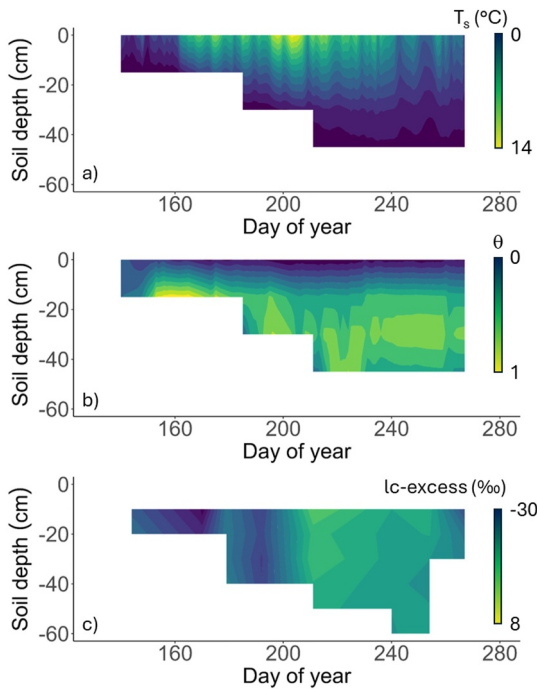


Figure 11. Soil conditions and isotopic states in 2019; soil conditions including soil temperature (T_s , °C), soil moisture fraction (θ) and lc-excess (‰) (top to bottom). As with Figures 9 and 10, the absence of data below the contour plots implies the presence of frozen ground and the lower edge of the plots approximates the frost table depth as soils were sampled only down to the frost table.

et al., 2001; Nicholls & Carey, 2021). Bowen ratios are similar to those documented in other Canadian Shield locations (Amiro & Wuschke, 1987; Fitzjarrald & Moore, 1994; Spence & Rouse, 2002). Sparse stand r_c was high compared to the $\sim 300 \text{ s m}^{-1}$ estimated from sites in northern Quebec (Fitzjarrald & Moore, 1994), but lower than the $\sim 500 \text{ s m}^{-1}$ observed at a site further north in the Northwest Territories (Spence & Rouse, 2002). Values of α were well below 1.26 (Table 3) which is common in these types of boreal forest canopies (Eugster et al., 2000). Surface resistance had to be less than 175 and 243 s m^{-1} at dense and sparse sites, respectively, to result in α values above 1.26. These r_c thresholds are higher than those documented by McNaughton and Spriggs (1989) in a wetter temperate setting, perhaps suggesting that equilibrium evaporation occurs despite higher resistance. This may be an artifact of the relatively sparse canopies. There was less interannual variability in dense canopy ET than in the sparse canopy. During the drier 2019, when rainfall averaged 106 mm lower than 2018 and 2020, evapotranspiration in the dense stand declined by 8 mm (4%). The decrease over the sparse canopy was 20 mm (15%). It is apparent that greater forest density imparts increased stability in evapotranspiration through wet and dry years.

Ω represents energy partitioning behavior and explains why the dense canopy exhibited less variability in Q_e . The very small Ω and α values in the sparse stand suggest ET there is driven more by atmospheric conditions and physiological response (e.g., VPD) than radiation, resulting in a more dynamic evapotranspirative response. This behavior is aligned with Iida et al. (2009) who found comparable results in a taiga canopy in eastern Siberia with a comparable tree density to that of the sparse canopy forest. The dense canopy forest, on the other hand, had a higher Ω , lower r_c and tended to be more freely evapotranspiring. The slightly higher slope of the $\Omega * Q_e(\text{eq}) - Q_e$ curve in the denser forest (0.27 vs. 0.18) also supports the idea of more freely evapotranspiring canopy with increased density. Nakai et al. (2013), too, observed that tree infilling reduces roughness and dry air movement to the understory with a commensurate increase in Ω . Beringer et al. (2005) found Q^* becomes larger and more important for ET with tree density as Ω increases. Because of this higher sensitivity to radiative drivers (Figure 5), and more consistent net radiation year-to-year (Table 3; Figure 3) than r_c (Table 3; Figure 4) the dense stand exhibited less variability in Q_e . Thus, an increase in forest density could result in more consistency in annual ET over the catchment. These results support those of Jarvis and McNaughton (1986) who showed Ω will always be larger for more extensive canopies than for isolated individuals. Each canopy was coupled differently with the atmosphere which influenced energy partitioning, turbulent flux behavior and ET (conceptually illustrated in Figure 12). The variation in Ω with wetness, particularly in the dense stand, has been documented before (Hadiwijawa et al., 2020) and reflects altered sources of transpiration (over vs. understory) and evaporation (intercepted water and forest floor). This implies a change in the main source of transpiration with wetness that could alter vegetation water use and vadose zone hydrology.

transpiring canopy with increased density. Nakai et al. (2013), too, observed that tree infilling reduces roughness and dry air movement to the understory with a commensurate increase in Ω . Beringer et al. (2005) found Q^* becomes larger and more important for ET with tree density as Ω increases. Because of this higher sensitivity to radiative drivers (Figure 5), and more consistent net radiation year-to-year (Table 3; Figure 3) than r_c (Table 3; Figure 4) the dense stand exhibited less variability in Q_e . Thus, an increase in forest density could result in more consistency in annual ET over the catchment. These results support those of Jarvis and McNaughton (1986) who showed Ω will always be larger for more extensive canopies than for isolated individuals. Each canopy was coupled differently with the atmosphere which influenced energy partitioning, turbulent flux behavior and ET (conceptually illustrated in Figure 12). The variation in Ω with wetness, particularly in the dense stand, has been documented before (Hadiwijawa et al., 2020) and reflects altered sources of transpiration (over vs. understory) and evaporation (intercepted water and forest floor). This implies a change in the main source of transpiration with wetness that could alter vegetation water use and vadose zone hydrology.

4.2. Vegetation Water Use

During much of the growing season, vegetation isotopic signatures plotted on or near the LMWL, much like results from the same species in the southern boreal forest (Nehemy et al., 2022) or similar pine forests in Scotland (Geris et al., 2015). Early in the season, lower, more negative values of $\delta^2\text{H}$ in plant water suggests vegetation accesses snowmelt (Figure 6), comparable to the findings of Nehemy et al. (2022). The shallow (<20 cm) rooting depths of both over and understory species (Finger et al., 2016; Gale & Grigal, 1987) is a probable explanation, as is the necessarily shallow early season frost table (Figure 9). By mid summer (i.e., July) values of $\delta^2\text{H}$ in plant water increased and lc-excess became less negative (Figure 7), suggesting that at this time vegetation, independent of canopy density or species, tends to use younger soil moisture derived from rainfall rather than any remaining snowmelt stored in the soil, if the former is available. The non-linear relationships between 7-, 14-, and 30-day rainfall and lc-excess values in vegetation imply that plants use younger water most of the year and only access older, more evaporatively enriched soil water with deeper roots or ectomycorrhizae when rainfall is

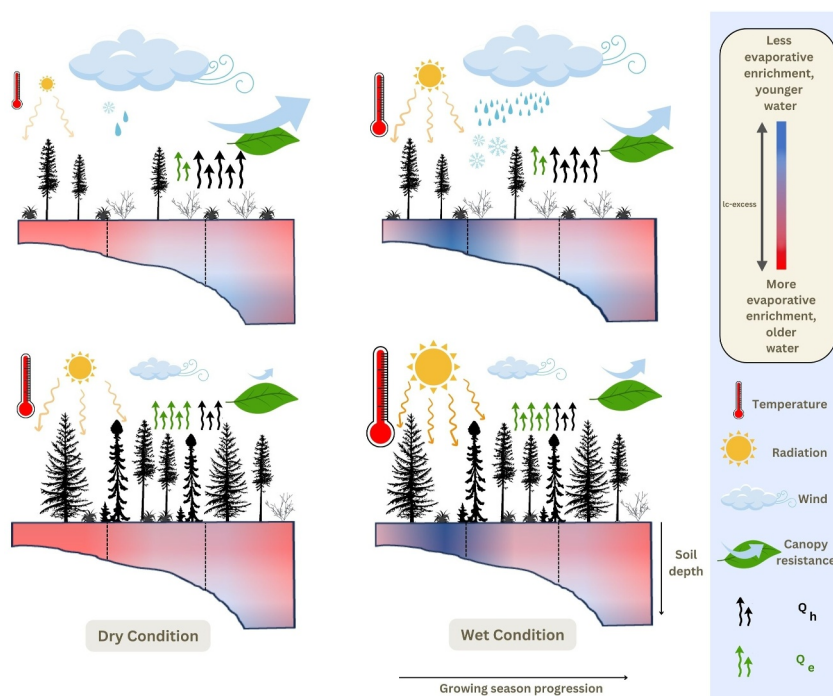


Figure 12. Conceptual diagram of differences in energy partitioning, vegetation water use and soil state within dense and sparse canopies under different wetness conditions in the subarctic Canadian Shield. The width of the flux arrows denotes the magnitude of the flux. Dry conditions (denoted by fewer raindrops and snowflakes) are portrayed in the left column and wet conditions (more raindrops and snowflakes) in the right column. Sparse canopies are illustrated in the top panels and dense canopies in the bottom panels (denoted by relatively more plants). The relative magnitudes of the turbulent fluxes are reflected in the widths of the black (Q_h) and green (Q_e) arrows. The relative influence of atmospheric conditions (air temperature, net radiation, wind speed and canopy resistance) are denoted by their relative sizes (e.g., net radiation and air temperature are more influential over denser canopies). In the soil column, the lower boundary reflects the depth of the frost table as the growing season progresses. Bluer tones are indicative of younger less evaporatively enriched water. Red tones; older, more evaporatively enriched water. The three soil water phases discussed in the text are denoted by the vertical black lines in the soil profiles, exemplified in the upper right panel when the first phase ends when ample new rain is introduced. The third phase begins with senescence, at which time any new water that has escaped evapotranspiration has drained to lower depths, leaving more evaporatively enriched water near the surface.

lacking (Table 6). Both over and understory species access a variety of soil water sources during the growing season. The seasonal averages in Tables 4 and 6 suggest that there is a difference between soil and plant water which might imply a degree of ecohydrological separation (Brooks et al., 2015) in that plants are drawing water from sources different than those used to generate runoff. However, as pointed out by Nehemy et al. (2022), analysis at higher frequencies (Figure 7) reveals little difference between soil and plant water over shorter periods. The patterns observed here indicate that plants are merely behaving opportunistically (Nehemy et al., 2022; Nicholls & Carey, 2021) and the differences in seasonal averages are likely biased by observations at the beginning and end of each growing season.

Black spruce and tamarack have different water use strategies (Nehemy et al., 2022; J. M. Warren et al., 2021). However, neither stem water $\delta^2\text{H}$ nor lc -excess values were significantly different between these two species (Figures 6 and 7; Table 4). Compared to tamarack and jack pine, black spruce demonstrate greater stomatal regulation in response to warming and drying, (Dang et al., 1997; Dusenge et al., 2021; J. M. Warren et al., 2021). Black spruce are also believed to have a greater ability to extract water from the soil compared to jack pine (Dang et al., 1997). However, even if canopy composition changes, the broad similarities across species in the timing and source of water they use suggests the impact of compositional changes may be limited. That said, with variation in moisture and temperature, differences between ET rates in the two stands became apparent. Evapotranspiration during dry conditions in the dense stand did not decline as much as that of the sparse stand. There was a tendency for plants to use older soil water when conditions were drier, which was reflected in lower lc -excess values in 2019 among all species (Table 4). If denser stands result in higher, more stable ET rates overall, as suggested by

the eddy covariance measurements, especially in dry years, this would have implications for the age of water that remains in the soil as canopies become denser.

4.3. Soil Water State

If effective precipitation (i.e., P minus ET) were constant through time, then there would be little change in the relative proportions of water of different lc -excess signatures stored in the catchment (Hrachowitz et al., 2016). The strong seasonality observed (Figures 7 and 9) is indicative of how the age of water stored below each canopy varies, because of differences in rates of ET as P was similar at the two stands. The water remaining in the soil is an amalgamation of all the fluxes over time (Tetzlaff et al., 2021). The variety in lc -excess caused by the interplay between ET and P complements findings elsewhere in northern temperate and boreal forests (Hrachowitz et al., 2016; Nehemy et al., 2022; Penna et al., 2018; Sprenger, Tetzlaff, Buttle, Carey, et al., 2018). The isotopic signatures in soil water suggest there can be three phases that comprise each growing season, with the beginning and end of each defined by a function of wetness conditions (Figure 12). The first phase follows snowmelt and leaf-out, where in the absence of rain, the soil steadily warms and dries (Figures 10–12). During this phase, the soil column contains water that is becoming evaporatively enriched with more negative values of lc -excess (Figures 9 and 12). Early in the growing season the shallow frost table keeps water near the surface, preventing water from draining to deeper layers and mixing with antecedent waters until later in the season. Thus, when frost tables are shallow, there is enhanced enrichment of water with heavier isotopes, particularly in dry years (e.g., 2019 in Figures 7 and 10).

Rain, if ample, can add water enriched in δ^2H and $\delta^{18}O$ to the soil column beginning the second phase, making lc -excess less negative (e.g., 2018 and 2020, Figures 7b, 9, and 10). This mixing of antecedent and new water creates variation in water ages in the soil column, reflected in patterns of lc -excess values (Figures 7 and 9). For example, at a catchment in the southern Yukon, soil water enrichment in heavier isotopes only occurred in shallow soils and suggested there is a threshold depth at which values remain on the LMWL (Shatilla, 2020). At Baker Creek, in 2018 and 2020, seasonal lc -excess values indicate shallow soils became evaporatively enriched relative to deeper soils (Table 4). In 2019, this pattern was particularly evident as the dry conditions resulted in more negative seasonal lc -excess values. McCutcheon et al. (2017) also found soil water isotopic signature variation with soil depth and season depends on the amount of water available. In contrast to their results, which may be a function of climate, soils (<50 cm) in the subarctic have less negative lc -excess values in wetter years, and a lack of evaporative enrichment; this reverses in dry years. The diverse lc -excess values in the 3 years of observation reveals the role of rainfall amounts and timing. This was especially evident in the dense canopy where growing season ET was less sensitive to moisture conditions. The final phase occurs at the very end of the growing season as evapotranspiration rates decrease with leaf senescence and winter dormancy. Any rainfall at this time of year increases lc -excess signatures in soil water. However, this water will freeze in place if storage thresholds for runoff production are not exceeded (Spence & Woo, 2003) and become subject to evaporative enrichment early in the following growing season.

When there is lower ET in the sparse stand, storage remains higher. The relatively lower ET rates result in soil water that remains less evaporatively enriched (less negative lc -excess). This implies that there is an inverse storage effect (Harman, 2015) in the soil beneath subarctic canopies, in that wetter soils are dominated by younger water. More rainfall also leads to this condition (Figures 9 and 10). Wetter conditions lead to more water held in storage, reducing water ages and soil column travel times, particularly in sparser stands. This effect has been simulated with models of water residence time in small catchments in the boreal forests of Krycklan, Sweden (Sprenger, Tetzlaff, Buttle, Laudon, & Soulsby, 2018). Sniderhan et al. (2023) documented a trend toward denser forest canopies across the Baker Creek catchment between 1972 and 2017. The results here imply this trend will be associated with increased water residence times in the soils in this landscape.

4.4. Implications at the Catchment Scale

The catchment land cover distribution of the Baker Creek catchment is dominated by two types—exposed bedrock and open water. These two types comprise 62% of the catchment, which is representative of much of the subarctic Canadian Shield landscape. If we assume that tree infilling will predominantly take place only where soil is adequate for colonization of tree species (i.e., not exposed bedrock or water bodies), apply the average annual growing season ET measured from 2018 to 2020 over both canopies (Table 3) and pro-rate them for a scenario in which all sparse canopies are replaced with dense canopies, catchment scale ET increases by 11%. This is arguably

within the uncertainty of observations. There are markedly different seasonal ET rates between sparse and dense canopies in this landscape. However, there is not enough land into which trees can reasonably expand to create dense canopies and the difference between sparse and dense canopy ET not sufficiently different that changes would measurably alter the ET rate at catchment or landscape scales. The only force that might have the ability to alter vegetation distribution and composition at such a scale to shift catchment scale ET is wildfire (Baltzer et al., 2021; Spence et al., 2020).

This result is different than that suggested from studies in other ecozones that are experiencing widespread land cover change associated with climate change. For example, along the latitudinal treeline where vegetation change is not constrained by surficial geology, changes in vegetation canopies that may alter evapotranspiration regimes can extend across more of the landscape. While the results of Nicholls and Carey (2021) suggest that catchment ET should increase as shrubs and trees expand altitudinally, the portion of land available above the existing treeline will influence how much of an impact tree expansion will have in mountainous landscapes. This limitation should be less apparent at the latitudinal treeline where land is widely available.

The Taiga Shield in northwestern Canada exhibits strong wet and dry cycles (Spence & Rausch, 2005). Superimposed on this has been a strong increasing trend (20% over the last half century) in annual precipitation (Zhang et al., 2019). Soil moisture state is important for runoff production in this landscape (Spence & Woo, 2003) and catchment scale runoff depends on how often and by how much precipitation can offset ET. During periods of drought, catchments may become more prone to periods of low flows as higher ET from denser forests results in fewer instances of exceedance of storage thresholds that govern runoff generation. During wet phases, runoff production will thus depend on the seasonality of enhanced precipitation (i.e., snowmelt vs. rainfall). The impact of a tendency toward older water in the soil column on aquatic chemistry will depend on this precipitation seasonality and when hillslopes are activated and become hydrologically connected to the stream (Oswald & Branfireun, 2014; Spence et al., 2015).

5. Conclusions

The objectives of this research were to answer two questions; (a) how does canopy density in the Taiga Shield influence (a) energy partitioning, (b) vegetation water use, and (c) soil water state (i.e., age and moisture), as well as (b) how much canopy densification is needed to create measurable changes in ET at the catchment scale? While most available energy was partitioned into sensible heat, latent heat fluxes were consistently higher in the denser canopy than the sparse. As with many subarctic landscapes, the influence of aerodynamic controls was higher than radiative controls, but canopies are more sensitive to changes in radiative inputs, and this was the case with the dense canopy. All sampled vegetation species tended to be opportunistic in their water use, accessing shallow soil water. Only when conditions were dry did vegetation access deeper older water sources more evaporatively enriched in heavier isotopes. The result is that the isotopic signature of the water in the soil profile was a complex mixture that depended on when water was added and removed. Sparse canopies tended to have wetter soil moisture states and soil water that resembles younger, heavier water sources (i.e., rainfall) enriched in $\delta^2\text{H}$ and $\delta^{18}\text{O}$. These differences imply that densification of the tree canopy could have implications for aquatic chemistry as soil water residence times will change. However, catchment and landscape scale ET rates in the subarctic Canadian Shield landscape are likely to be generally insensitive to these changes as the magnitude of the differences between the sparse and dense canopy were relatively small and the presence of exposed bedrock and the numerous lakes reduce the portion of the landscape that is subject to tree infilling. This demonstrates the importance of surficial geology for larger scale impacts of climate induced vegetation change. Implications of changing residence times of soil water on runoff generation and aquatic chemistry because of tree infilling are less obvious. They may be a function of the frequency of wet and dry cycles in precipitation and the relative rates of P and enhanced ET over denser forests as this controls when runoff generation thresholds are exceeded.

Data Availability Statement

Data used in this study (Environment and Climate Change Canada, 2024) are available from Environment and Climate Change Canada's Data Catalogue (Baker Creek Research Watershed Ecohydrology Data 2018 to 2020 - ECCDC Data Catalogue). Environment and Climate Change Canada station Yellowknife A meteorological data used

within the study (Environment and Climate Change Canada, 2023) are available from <https://open.canada.ca/data/en/dataset/9c4ebc00-3ea4-4fe0-8bf2-66cfe1cddd1d>.

Acknowledgments

The authors would like to thank Newell Hedstrom, Cuyler Onclin, Mark Russell and Jason Friesen of Environment and Climate Change Canada for their leadership coordinating field operations at the Baker Creek Research Watershed. The Department of Environment and Climate Change of the Government of the Northwest Territories also provided in-kind support. Funding for this project was provided by Environment and Climate Change Canada, Northern Water Futures (a Global Water Futures project) and the Natural Sciences and Engineering Research Council. JLB and OS are supported by the Canada Research Chairs program. Thank you to Christina Tjandra for drafting Figure 11.

References

- Amiro, B. D., & Wuschke, E. E. (1987). Evapotranspiration from a boreal forest drainage basin using an energy balance/eddy correlation technique. *Boundary-Layer Meteorology*, 38(1–2), 125–139. <https://doi.org/10.1007/bf00121560>
- Bailey, W. G., & Davies, J. A. (1981). Bulk stomatal resistance control on evaporation. *Boundary-Layer Meteorology*, 20(4), 401–415. <https://doi.org/10.1007/bf00122291>
- Baldocchi, D., Kelliher, F. M., Black, T. A., & Jarvis, P. (2000). Climate and vegetation controls on boreal zone energy exchange. *Global Change Biology*, 6(S1), 69–83. <https://doi.org/10.1046/j.1365-2486.2000.06014.x>
- Baltzer, J. L., Day, N. J., Walker, X. J., Greene, D., Mack, M. C., Alexander, H. D., et al. (2021). Increasing fire and the decline of fire adapted black spruce in the boreal forest. *Proceedings of the National Academy of Science*, 118(45), e2024872118. <https://doi.org/10.1073/pnas.2024872118>
- Beringer, J., Chapin, III, F. S., Thompson, C. C., & McGuire, A. D. (2005). Surface energy exchanges along a tundra-forest transition and feedbacks to climate. *Agricultural and Forest Meteorology*, 131(3–4), 143–161. <https://doi.org/10.1016/j.agrformet.2005.05.006>
- Blanken, P. D., Black, T. A., Neumann, H. H., den Hartog, G., Yang, P. C., Nesic, Z., & Lee, X. (2001). The seasonal water and energy exchange above and within a boreal aspen forest. *Journal of Hydrology*, 245(1–4), 118–136. [https://doi.org/10.1016/s0022-1694\(01\)00343-2](https://doi.org/10.1016/s0022-1694(01)00343-2)
- Bonan, G. B. (2008). Forests and climate change: Forcings, feedbacks, and the climate benefits of forests. *Science*, 320(5882), 1444–1449. <https://doi.org/10.1126/science.1155121>
- Botter, G., Bertuzzo, E., & Rinaldo, A. (2010). Transport in the hydrologic response: Travel time distributions, soil moisture dynamics, and the old water paradox. *Water Resources Research*, 46(3), W03514. <https://doi.org/10.1029/2009wr008371>
- Box, J. E., Colgan, W. T., Christensen, T. R., Schmidt, N. M., Lund, M., Parmentier, F.-J. W., et al. (2019). Key indicators of Arctic climate change: 1971–2017. *Environmental Research Letters*, 14(4), 045010. <https://doi.org/10.1088/1748-9326/aafcb1b>
- Brooks, P. D., Chorover, J., Fan, Y., Godsey, S. E., Maxwell, R. M., McNamara, J. P., & Tague, C. (2015). Hydrological partitioning in the critical zone: Recent advances and opportunities for developing transferable understanding of water cycle dynamics. *Water Resources Research*, 51(9), 6973–6987. <https://doi.org/10.1002/2015WR017039>
- Chapin, III, F. S., Sturm, M., Serreze, M. C., McFadden, J. P., Key, J. R., Lloyd, A. H., et al. (2005). Role of land surface changes in arctic summer warming. *Science*, 310(5748), 657–660. <https://doi.org/10.1126/science.1117368>
- Charuchittipan, D., Bahel, W., Mauder, M., Leps, J.-P., & Folken, T. (2014). Extension of the averaging time in eddy covariance measurements and its effects on the energy balance closure. *Boundary-Layer Meteorology*, 152(3), 303–327. <https://doi.org/10.1007/s10546-014-9922-6>
- Dang, Q.-L., Margolis, H. A., Coyea, M. R., Sy, M., & Collatz, G. J. (1997). Regulation of branch-level gas exchange of boreal trees: Roles of shoot water potential and vapor pressure difference. *Tree Physiology*, 17(8–9), 521–535. <https://doi.org/10.1093/treephys/17.8-9.521>
- Dusenage, M. E., Ward, E. J., Warren, J. M., Stinziano, J. R., Wullschlegel, S. D., Hanson, P. J., & Way, D. A. (2021). Warming induces divergent stomatal dynamics in co-occurring boreal trees. *Global Change Biology*, 27(13), 3079–3094. <https://doi.org/10.1111/gcb.15620>
- Eaton, A. K., Rouse, W. R., Lafleur, P. M., Marsh, P., & Blanken, P. D. (2001). Surface energy balance of the western and central Canadian subarctic: Variations in the energy balance among five major terrain types. *Journal of Climate*, 14(17), 3692–3703. [https://doi.org/10.1175/1520-0442\(2001\)014<3692:sebotw>2.0.co;2](https://doi.org/10.1175/1520-0442(2001)014<3692:sebotw>2.0.co;2)
- Elmendorf, S., Henry, G., Hollister, R., Björk, R. G., Boulanger-Lapointe, N., Cooper, E. J., et al. (2012). Plot-scale evidence of tundra vegetation change and links to recent summer warming. *Nature Climate Change*, 2(6), 453–457. <https://doi.org/10.1038/nclimate1465>
- Endrizzi, S., & Marsh, P. (2010). Observations and modelling of turbulent fluxes during melt at the shrub tundra transition zone 1: Point scale variations. *Hydrology Research*, 41(6), 471–491. <https://doi.org/10.2166/nh.2010.149>
- Environment and Climate Change Canada. (2023). *Canadian Climate Normals*. Government of Canada. Retrieved from https://climate.weather.gc.ca/climate_normals/index_e.html
- Environment and Climate Change Canada. (2024). Baker Creek Research Watershed Ecohydrology Data 2018 to 2020. Retrieved from <https://catalogue.ec.gc.ca/geonetwork/srv/eng/catalog.search#/home>
- Epstein, S., & Mayeda, T. (1953). Variation of ¹⁸O content of waters from natural sources. *Geochimica et Cosmochimica Acta*, 4(5), 213–224. [https://doi.org/10.1016/0016-7037\(53\)90051-9](https://doi.org/10.1016/0016-7037(53)90051-9)
- Eugster, W., Rouse, W. R., Pielke, R. A., McFadden, J. P., Baldocchi, D., Kittel, T. G. F., et al. (2000). Land atmosphere energy exchange in Arctic tundra and boreal forest: Available data and feedbacks to climate. *Global Change Biology*, 6(S1), 84–115. <https://doi.org/10.1046/j.1365-2486.2000.06015.x>
- Finger, R. A., Turetsky, M. R., Kielland, K., Ruess, R. W., Mack, M. C., & Euskirchen, E. S. (2016). Effects of permafrost thaw on nitrogen availability and plant-soil interactions in a boreal Alaskan lowland. *Journal of Ecology*, 104(6), 1542–1554. <https://doi.org/10.1111/1365-2745.12639>
- Fitzjarrald, D. R., & Moore, K. E. (1994). Growing season boundary layer climate and surface exchanges in a subarctic lichen woodland. *Journal of Geophysical Research*, 99(D1), 1899–1917. <https://doi.org/10.1029/93jd01019>
- Foster, A. C., Wang, J. A., Frost, G. V., Davidson, S. J., Hoy, E., Turner, K. W., et al. (2022). Disturbances in North American boreal forest and Arctic tundra: Impacts, interactions, and responses. *Environmental Research Letters*, 17(11), 113001. <https://doi.org/10.1088/1748-9326/ac98d7>
- Gale, M. R., & Grigal, D. F. (1987). Vertical root distributions of northern tree species in relation to successional status. *Canadian Journal of Forest Research*, 17(8), 829–834. <https://doi.org/10.1139/x87-131>
- Garratt, J. R. (1994). Review: The atmospheric boundary layer. *Earth-Science Reviews*, 37(1–2), 89–134. [https://doi.org/10.1016/0012-8252\(94\)90026-4](https://doi.org/10.1016/0012-8252(94)90026-4)
- Geris, J., Tetzlaff, D., McDonnell, J. J., Anderson, J., Paton, G., & Soulsby, C. (2015). Ecohydrology separation in wet, low energy northern environments? A preliminary assessment using soil water extraction techniques. *Hydrological Processes*, 29(25), 5139–5152. <https://doi.org/10.1002/hyp.10603>
- Geris, J., Tetzlaff, D., McDonnell, J. J., & Soulsby, C. (2017). Spatial and temporal patterns of soil water storage and vegetation water use in humid northern catchments. *Science of the Total Environment*, 595, 486–493. <https://doi.org/10.1016/j.scitotenv.2017.03.275>
- Gibson, J. J., & Reid, R. (2010). Stable isotope fingerprint of open water evaporation losses and effective drainage area fluctuations in a subarctic shield watershed. *Journal of Hydrology*, 381(1–2), 142–150. <https://doi.org/10.1016/j.jhydrol.2009.11.036>

- Gibson, J. J., Reid, R., & Spence, C. (1998). A six-year isotopic record of lake evaporation in the Canadian subarctic. *Hydrological Processes*, 12, 1779–1992.
- Grelle, A., Lundberg, A., Lindroth, A., Morén, A.-S., & Cienciala, E. (1997). Evaporation components of a boreal forest: Variations during the growing season. *Journal of Hydrology*, 197(1–4), 70–87. [https://doi.org/10.1016/S0022-1694\(96\)03267-2](https://doi.org/10.1016/S0022-1694(96)03267-2)
- Gröning, M., Lutz, H. O., Roller-Lutz, Z., Kralik, M., Gourcy, L., & Pöhlstein, L. (2012). A simple rain collector preventing water re-evaporation dedicated for $\delta^{18}\text{O}$ and $\delta^2\text{H}$ analysis of cumulative precipitation samples. *Journal of Hydrology*, 448–449, 195–200. <https://doi.org/10.1016/j.jhydrol.2012.04.041>
- Hadiwijawa, B., Pepin, S., Isabelle, P.-E., & Nadeau, D. F. (2020). The dynamics of transpiration to evapotranspiration ratio under wet and dry canopy conditions in a humid boreal forest. *Forests*, 11(2), 237. <https://doi.org/10.3390/f11020237>
- Halldin, S., Grip, H., Jansson, P. E., & Lindgren, A. (1980). Micrometeorology and hydrology of pine forest ecosystems II, Theory and models. In T. Persson (Ed.), *Structure and Function of Northern Coniferous Forests—An Ecosystem Study, Ecological Bulletins* (Vol. 32, pp. 463–503).
- Harman, C. J. (2015). Time-variable transit time distributions and transport: Theory and application to storage-dependent transport of chloride in a watershed. *Water Resources Research*, 51(1), 1–30. <https://doi.org/10.1002/2014WR015707>
- Heim, R. J., Bucharova, A., Brodt, L., Kamp, J., Rieker, D., Soromotin, A. V., et al. (2021). Post-fire vegetation succession in the Siberian subarctic tundra over 45 years. *Science of The Total Environment*, 760, 143425. <https://doi.org/10.1016/j.scitotenv.2020.143425>
- Helbig, M., Wishniewski, K., Kljun, N., Chasmer, L. E., Quinton, W. L., Detto, W. L., & Sonnentag, O. (2016). Regional atmospheric cooling and wetting effect of permafrost thaw-induced boreal forest loss. *Global Change Biology*, 22(12), 4048–4066. <https://doi.org/10.1111/gcb.13348>
- Hendry, M. J., Schmeling, E., Wassenaar, L. I., Barbour, S. L., & Pratt, D. (2015). Determining the stable isotope composition of pore water from saturated and unsaturated zone core: Improvements to the direct vapour equilibration laser spectrometry method. *Hydrology and Earth System Sciences*, 19(11), 4427–4440. <https://doi.org/10.5194/hess-19-4427-2015>
- Hollander, M., & Wolfe, D. A. (1973). *Nonparametric statistical methods*. John Wiley & Sons.
- Horst, T. W. (1997). A simple formula for attenuation of eddy fluxes measured with first order response scalar sensors. *Boundary-Layer Meteorology*, 94(3), 517–520. <https://doi.org/10.1023/a:1002427517744>
- Hrachowitz, M., Benettin, P., van Breukelen, B. M., Fovet, O., Howden, N. J. K., Ruiz, L., et al. (2016). Transit times – The link between hydrology and water quality at the catchment scale. *WIREs Water*, 3(5), 629–657. <https://doi.org/10.1002/wat2.1155>
- Iida, S., Ohta, T., Matsumoto, K., Nakai, T., Kuwada, T., Kononov, A. V., et al. (2009). Evapotranspiration from understory vegetation in an eastern Siberian boreal larch forest. *Agricultural and Forest Meteorology*, 149(6–7), 1129–1139. <https://doi.org/10.1016/j.agrformet.2009.02.003>
- Jarvis, P. G., & McNaughton, K. G. (1986). Stomatal control of transpiration: Scaling up from leaf to region. In *Advances in Ecological Research* (Vol. 15, pp. 1–49). Academic Press. [https://doi.org/10.1016/S0065-2504\(08\)60119-1](https://doi.org/10.1016/S0065-2504(08)60119-1)
- Jorgenson, M. T., Shur, Y. L., & Osterkamp, T. E. (2008). Thermokarst in Alaska. In *Proceedings of the Ninth International Conference on Permafrost* (Vol. 29, pp. 869–876). Institute of Northern Engineering, University of Alaska Fairbanks.
- Kaimal, J. C., & Finnigan, J. J. (1994). *Atmospheric boundary layer flows – Their structure and measurement*. Oxford University Press.
- Kasurinen, V., Alfredsen, K., Kolari, P., Mammarella, I., Alekseychik, P., Rinne, J., et al. (2014). Latent heat exchange in the boreal and arctic biomes. *Global Change Biology*, 20(11), 3439–3456. <https://doi.org/10.1111/gcb.12640>
- Kettridge, N., Thompson, D. K., Bombonato, L., Turetsky, M. R., Benscoter, B. W., & Waddington, J. M. (2013). The ecohydrology of forested peatlands: Simulating the effects of tree shading on moss evaporation and species composition. *Journal of Geophysical Research: Biogeosciences*, 118(2), 422–435. <https://doi.org/10.1002/jgrg.20043>
- Kljun, N., Calanca, P., Rotach, M. W., & Schmid, H. P. (2015). A simple two-dimensional parameterization for flux footprint prediction (FFP). *Geoscientific Model Development*, 8(11), 3695–3713. <https://doi.org/10.5194/gmd-8-3695-2015>
- Koeniger, P., Marshall, J. D., Link, T., & Mulch, A. (2011). An inexpensive, fast, and reliable method for vacuum extraction of soil and plant water for stable isotope analyses by mass spectrometry. *Rapid Communication Mass Spectrometry*, 25(20), 3041–3048. <https://doi.org/10.1002/rcm.5198>
- Kokelj, S. V., Gingras-Hill, T., Daly, S. V., Morse, P., Wolfe, S., Rudy, A. C. E., et al. (2023). The Northwest Territories Thermokarst Mapping Collective: A northern-driven mapping collaborative toward understanding the effects of permafrost thaw. *Arctic Science*. (in press). <https://doi.org/10.1139/as-2023-0009>
- Lafleur, P. M. (1992). Energy balance and evapotranspiration from a subarctic forest. *Agricultural and Forest Meteorology*, 58(3–4), 163–175. [https://doi.org/10.1016/0168-1923\(92\)90059-d](https://doi.org/10.1016/0168-1923(92)90059-d)
- Lafleur, P. M., & Humphreys, E. R. (2018). Tundra shrub effects on growing season energy and carbon dioxide exchange. *Environmental Research Letters*, 13(5), 055001. <https://doi.org/10.1088/1748-9326/aab863>
- Landwehr, J. M., & Coplen, T. B. (2006). Line-conditioned excess: A new method for characterizing stable hydrogen and oxygen isotope ratios in hydrologic systems. In *International Conference on Isotopes in Environmental Studies, Aquatic Forum, Monte-Carlo, Monaco, 25–29 October 2004* (pp. 132–135). IAEA.
- Lantz, T. C., Marsh, P., & Kokelj, S. V. (2013). Recent shrub proliferation in the Mackenzie Delta uplands and microclimatic implications. *Ecosystems*, 16(1), 47–59. <https://doi.org/10.1007/s10021-012-9595-2>
- Martínez-Cob, A., & Suvočarev, K. (2015). Uncertainty due to hygrometer sensor in eddy covariance latent heat flux measurements. *Agricultural and Forest Meteorology*, 200, 92–96. <https://doi.org/10.1016/j.agrformet.2014.09.021>
- Massman, W. J. (2000). A simple method for estimating frequency response corrections for eddy covariance systems. *Agricultural and Forest Meteorology*, 104(3), 185–198. [https://doi.org/10.1016/S0168-1923\(00\)00164-7](https://doi.org/10.1016/S0168-1923(00)00164-7)
- Mauder, M., Oncley, S. P., Woft, R., Weidinger, T., Riberio, L., Bernhofer, C., et al. (2007). The energy balance experiment EBEX-2000. Part II: Intercomparison of eddy-covariance sensors and post-field data processing methods. *Boundary-Layer Meteorology*, 123(1), 29–54. <https://doi.org/10.1007/s10546-006-9139-4>
- McCutcheon, R. J., McNamara, J. P., Kohn, M. J., & Evans, S. L. (2017). An evaluation of the ecohydrological separation hypothesis in a semiarid catchment. *Hydrological Processes*, 31(4), 783–799. <https://doi.org/10.1002/hyp.11052>
- McDonnell, J. J. (2014). The two water worlds hypothesis: Ecohydrological separation of water between streams and trees? *WIREs Water*, 1(4), 323–329. <https://doi.org/10.1002/wat2.1027>
- McDowell, N., Pockman, W. T., Allen, C. D., Breshears, D. D., Cobb, N., Kolb, T., et al. (2008). Mechanisms of plant survival and mortality during drought: Why do some plants survive while others succumb to drought? *New Phytologist*, 178(4), 719–739. <https://doi.org/10.1111/j.1469-8137.2008.02436.x>
- McNaughton, K. G., & Spriggs, T. W. (1989). An evaluation of the Priestley and Taylor equation and the complementary relationship using results from a mixed-layer model of the convective boundary layer. In *Estimation of Areal Evapotranspiration, Proceedings of a workshop held at Vancouver, BC, Canada, August 1987* (Vol. 177, pp. 89–104). IAHS Publication.

- Morrison, J., Brockwell, T., Merren, T., Fourel, F., & Phillips, A. M. (2001). On-line high-precision stable hydrogen isotopic analyses on nanoliter water samples. *Analytical Chemistry*, 73(15), 3570–3575. <https://doi.org/10.1021/ac001447t>
- Morse, P. D., Wolfe, S. A., Kokelj, S. V., & Gaanderse, A. J. R. (2015). The occurrence and thermal disequilibrium state of permafrost in forest ecotopes of the Great Slave Region, Northwest Territories, Canada. *Permafrost and Periglacial Processes*, 27(2), 145–162. <https://doi.org/10.1002/ppp.1858>
- Muggeo, V. M. R. (2008). Segmented: An R package to fit regression models with broken-line relationships. *R News*, 8(1), 20–25.
- Nakai, T., Kim, Y., Busey, R. C., Suzuki, R., Nagai, S., Kobayashi, H., et al. (2013). Characteristics of evapotranspiration from a permafrost black spruce forest in interior Alaska. *Polar Science*, 7(2), 136–148. <https://doi.org/10.1016/j.polar.2013.03.003>
- Nehemy, M. F., Benettin, P., Asadollahi, M., Pratt, D., Rinaldo, A., & McDonnell, J. J. (2021). Tree water deficit and dynamic source water partitioning. *Hydrological Processes*, 35(1), e14004. <https://doi.org/10.1002/hyp.14004>
- Nehemy, M. F., Mailliet, J., Perron, N., Pappas, C., Sonnentag, O., Baltzer, J. L., et al. (2022). Snowmelt water use at transpiration onset: Phenology, isotope tracing, and tree water transit time. *Water Resources Research*, 58(9), e2022WR032344. <https://doi.org/10.1029/2022WR032344>
- Nicholls, E. M., & Carey, S. K. (2021). Evapotranspiration and energy partitioning across a forest-shrub vegetation gradient in a subarctic, alpine catchment. *Journal of Hydrology*, 602, 126790. <https://doi.org/10.1016/j.jhydrol.2021.126790>
- Oke, T. R. (1987). *Boundary layer climates* (p. 435). Routledge.
- Oswald, C. J., & Branfireun, B. A. (2014). Antecedent moisture conditions control mercury and dissolved organic carbon concentration dynamics in a boreal headwater catchment. *Water Resources Research*, 50(8), 6610–6627. <https://doi.org/10.1002/2013WR014736>
- Penna, D., Hopp, L., Scandellari, F., Allen, S. T., Benettin, P., Beyer, M., et al. (2018). Ideas and perspectives: Tracing terrestrial ecosystem water fluxes using hydrogen and oxygen stable isotopes – Challenges and opportunities from an interdisciplinary perspective. *Biogeosciences*, 15(21), 6399–6415. <https://doi.org/10.5194/bg-15-6399-2018>
- Phillips, R. W., Spence, C., & Pomeroy, J. W. (2011). Connectivity and runoff dynamics in heterogeneous basins. *Hydrological Processes*, 25, 3061–3075. <https://doi.org/10.1002/hyp.8123>
- Priestley, C. H. B., & Taylor, R. J. (1972). On the assessment of surface heat flux and evaporation using large-scale parameters. *Monthly Weather Review*, 100(2), 81–92. [https://doi.org/10.1175/1520-0493\(1972\)100<0081:otaosh>2.3.co;2](https://doi.org/10.1175/1520-0493(1972)100<0081:otaosh>2.3.co;2)
- Reid, K. A., Reid, D. G., & Brown, C. D. (2021). Patterns of vegetation change in Yukon: Recent findings and future research in dynamic subarctic ecosystems. *Environmental Reviews*, 30(3), 380–401. <https://doi.org/10.1139/er-2021-0110>
- Shatilla, N. J. (2020). *New Insights into catchment dynamics using novel approaches* [PhD Thesis]. McMaster University.
- Snelgrove, J. R., Buttle, J. M., Kohn, M. J., & Tetzlaff, D. (2021). Co-evolution of xylem water and soil water stable isotopic composition in a northern mixed forest biome. *Hydrology and Earth System Science*, 25(4), 216–2186. <https://doi.org/10.5194/hess-25-2169-2021>
- Sniderhan, A. E., Spence, C., Kokelj, S. V., & Baltzer, J. L. (2023). Evidence for unexpected net permafrost aggradation driven by local hydrology and climatic triggers. *Environmental Research Letters*, 18(11), 115001. <https://doi.org/10.1088/1748-9326/acff0f>
- Spence, C., & Hedstrom, N. (2018). Hydrometeorological data from Baker Creek Research Watershed, Northwest Territories, Canada. *Earth System Science Data*, 10(4), 1753–1767. <https://doi.org/10.5194/essd-10-1753-2018>
- Spence, C., Hedstrom, N., Tank, S. E., Quinton, W. L., Olefeldt, D., Goodman, S., & Dion, N. (2020). Water budget resilience to forest fire in the subarctic Canadian Shield. *Hydrological Processes*, 34(25), 4940–4958. <https://doi.org/10.1002/hyp.13915>
- Spence, C., Kokelj, S. A., Kokelj, S. V., & Hedstrom, N. (2014). The process of winter streamflow generation in a subarctic Precambrian shield catchment. *Hydrological Processes*, 28(14), 2179–2190. <https://doi.org/10.1002/hyp.10119>
- Spence, C., Kokelj, S. V., Kokelj, S. A., McKluskie, M., & Hedstrom, N. (2015). Evidence of a change in water chemistry in Canada's subarctic associated with enhanced winter streamflow. *Journal of Geophysical Research: Biogeosciences*, 120(1), 113–127. <https://doi.org/10.1002/2014jg002809>
- Spence, C., & Rausch, J. (2005). Autumn synoptic conditions and rainfall in the subarctic Canadian Shield of the Northwest Territories, Canada. *International Journal of Climatology*, 25(11), 1493–1506. <https://doi.org/10.1002/joc.1185>
- Spence, C., & Rouse, W. R. (2002). The energy budget of subarctic Canadian Shield terrain and its impact on hillslope hydrology. *Journal of Hydrometeorology*, 3(2), 208–218. [https://doi.org/10.1175/1525-7541\(2002\)003<0208:tebocs>2.0.co;2](https://doi.org/10.1175/1525-7541(2002)003<0208:tebocs>2.0.co;2)
- Spence, C., & Woo, M. K. (2003). Hydrology of subarctic Canadian Shield: Soil-filled valleys. *Journal of Hydrology*, 279(1–4), 151–166. [https://doi.org/10.1016/s0022-1694\(03\)00175-6](https://doi.org/10.1016/s0022-1694(03)00175-6)
- Sprenger, M., Tetzlaff, D., Buttle, J., Carey, S. K., McNamara, J. P., Laudon, H., et al. (2018). Storage, mixing, and fluxes of water in the critical zone across northern environments inferred by stable isotopes of soil water. *Hydrological Processes*, 32(12), 1720–1737. <https://doi.org/10.1002/hyp.13135>
- Sprenger, M., Tetzlaff, D., Buttle, J., Laudon, H., & Soulsby, C. (2018). Water ages in the critical zone of long-term experimental sites in northern latitudes. *Hydrology and Earth System Science*, 22(7), 3965–3981. <https://doi.org/10.5194/hess-22-3965-2018>
- Sturm, M., Douglas, T., Racine, C., & Liston, G. E. (2005). Changing snow and shrub conditions affect albedo with global implications. *Journal of Geophysical Research*, 110(G1), G01004. <https://doi.org/10.1029/2005JG000013>
- Tetzlaff, D., Buttle, J., Carey, S. K., Kohn, M. J., Laudon, H., McNamara, J. P., et al. (2021). Stable isotopes of water reveal differences in plant – Soil water relationships across northern environments. *Hydrological Processes*, 35(1), e14023. <https://doi.org/10.1002/hyp.14023>
- Tetzlaff, D., Soulsby, C., Buttle, J., Capell, R., Carey, S. K., Laudon, H., et al. (2013). Catchments on the cusp? Structural and functional change in northern ecohydrology. *Hydrological Processes*, 27(5), 766–774. <https://doi.org/10.1002/hyp.9700>
- Thompson, D. K. (2012). *Wildfire impacts on peatland ecohydrology* [PhD Thesis]. McMaster University.
- Travers-Smith, H. Z., & Lantz, T. C. (2020). Leading-edge disequilibrium in alder and spruce populations across the forest–tundra ecotone. *Ecosphere*, 11(7), e03118. <https://doi.org/10.1002/ecs2.3118>
- Viereck, L. A., & Johnston, W. F. (1990). Picea mariana (Mill.) B. S. P. Black spruce. In R. Burns & B. Honkala (Eds.), *Silvics of North America, Conifers* (Vol. 1, pp. 227–237). USDA Forest Service Agriculture Handbook.
- Warren, J. M., Jensen, A. M., Ward, E. J., Guja, A., Childs, J., Wullschlegel, S. D., & Hanson, P. J. (2021). Divergent species-specific impacts of whole ecosystem warming and elevated CO₂ on vegetation water relations in an ombrotrophic peatland. *Global Change Biology*, 27(9), 1820–1835. <https://doi.org/10.1111/gcb.15543>
- Warren, R. K., Pappas, C., Helbig, M., Chasmer, L. E., Berg, A. A., Baltzer, J. L., et al. (2018). Minor contribution of overstory transpiration to landscape evapotranspiration in boreal permafrost peatlands. *Ecohydrology*, 11(5), e1975. <https://doi.org/10.1002/eco.1975>
- Wassenaar, L. I., Hendry, M. J., Chostner, V. L., & Lis, G. P. (2008). High resolution pore water δ²H and δ¹⁸O measurements by H₂O (liquid)–H₂O (vapor) equilibration laser spectroscopy. *Environmental Science & Technology*, 42(24), 9262–9267. <https://doi.org/10.1021/es802065s>
- Webb, E. K., Pearman, G. I., & Leuning, R. (1980). Correction of flux measurements for density effects due to heat and water vapour transfer. *Quarterly Journal of the Royal Meteorological Society*, 106(447), 85–100. <https://doi.org/10.1256/smsqj.44706>

- Wilcox, E. J., Wolfe, B. B., & Marsh, P. (2022). Assessing the influence of lake and watershed attributes on snowmelt bypass at thermokarst lakes. *Hydrology and Earth System Sciences*, 26(23), 6185–6205. <https://doi.org/10.5194/hess-26-6185-2022>
- Wright, S. N., Thompson, L. M., Olefeldt, D., Connon, R., Carpino, O. A., Beel, C. R., & Quinton, W. L. (2022). Thaw-induced impacts of land and water in discontinuous permafrost: A review of the Taiga Plains and Taiga Shield, northwestern Canada. *Earth-Science Reviews*, 232, 104104. <https://doi.org/10.1016/j.earscirev.2022.104104>
- Young-Robertson, J. M., Bolton, W. R., Bhatt, U. S., Cristobal, J., & Thoman, R. (2016). Deciduous trees are a large and overlooked sink for snowmelt water in the boreal forest. *Scientific Reports*, 6(1), 29504. <https://doi.org/10.1038/srep29504>
- Zhang, X., Flato, G., Kirchmeier-Young, M., Vincent, L., Wan, H., Wang, X., et al. (2019). Changes in temperature and precipitation across Canada; Chapter 4. In E. Bush & D. S. Lemmen (Eds.), *Canada's Changing Climate Report* (pp. 112–193). Government of Canada.